NASA Technical Memorandum X-73,239 AVRADCOM Technical Report 78-55 (AM)

(NASA-TM-X-73239) WIND-TUNNEL INVESTIGATION OF THE THRUST AUGMENTOR PERFORMANCE OF A LARGE-SCALE SWEPT WING MODEL (NASA) 58 p HC A04/MF A01 CSCL 01A
N79-17804
Unclas
G3/02 16318

Wind-Tunnel Investigation of the Thrust Augmentor Performance of a Large-Scale Swept Wing Model

David G. Koenig and Michael D. Falarski

February 1979

NASA
National Aeronautics and Space Administration

United States Army Aviation Research and Development Command

WIND-TUNNEL INVESTIGATION OF THE THRUST AUGMENTOR PERFORMANCE OF A LARGE-SCALE SWEPT WING MODEL

David G. Koenig
Ames Research Center

and

Michael D. Falarski
Ames Research Center
and
Aeromechanics Laboratory
AVRADCOM Research and Technology Laboratories

SUMMARY

Tests were made in the Ames 40- by 80-Foot Wind Tunnel to determine the forward speed effects on wing-mounted thrust augmentors. The large-scale model was that used in previous investigations and was powered by the compressor output of J-85 driven viper compressors. The flap settings used were 15° and 30° with 0°, 15° and 30° aileron settings. The maximum duct pressure, and wind-tunnel dynamic pressure were 66 cmHg (26 in Hg) and 1190 N/m^2 (25 lb/ft^2), respectively. All tests were made at zero sideslip. Test results are presented without analysis.

INTRODUCTION

Augmentor-wing research for use on STOL aircraft configurations has resulted in a series of large-scale static and wind-tunnel tests on a swept wing configuration. Overviews of this research have been published in references 1 and 2. Test results for the slotted primary nozzle are published in references 3 and 4 for the configuration to be referred to as 2 SW. Static gross augmentation was 1.27 at a pressure ratio of 1.7 for this slotted configuration.

To improve the augmentation ratio and to document thrust augmentation at airspeed, a series of static and wind-tunnel tests were made. As with previous tests this program was undertaken in cooperation with the Defense Research Board of Canada and De Havilland Aircraft of Canada, Limited. The tests included in the program were performed and reported in the following sequences.

Type of test and location	Configuration	Report
Static test, complete model, at Ames	4 SW cruciform nozzles	DHC DIR 74-1[a]
Static test semispan (cold air) at De Havilland	4 SW lobed nozzles	DHC-DIR 76[a]
Wind-tunnel test, Ames 40 by 80 test 460	4 SW	DHC 77-2[a]
Wind-tunnel test Ames 40 by 80 test 487	5 SW - nozzles same as 4 SW - nozzle fairing added (see fig. 3(f))	Present report and reference 5

[a]De Havilland reports

The results from the 4 SW tests may be obtained on request from either Ames or De Havilland and the data for the last tests are presented herein and in reference 5. The basic force and moment data are documented without analysis in this report. Flap and aileron deflections were limited to 15° and 30° in order to minimize profile drag due to flap deflection. For some tests, the shroud was removed with and without the augmentor vent sealed in order to simulate basic jet flap performance. In addition, tests were made with leading-edge slat deflection reduced and with slat removed in order to evaluate effects of possible flow separation on the slat lower surface.

SYMBOLS

b wing span, m (ft)

c chord, m (ft)

$\bar{c}$ mean aerodynamic chord, m (ft)

c_s wing leading-edge slat chord, m (ft)

C_d discharge coefficient (ratio of measured to calculated flow through the nozzle)

C_D drag coefficient, $\frac{\text{drag}}{qS}$

C_{D_m} total momentum drag coefficient, $\frac{\text{momentum drag}}{qS}$

C_{J_A} isentropic augmentor jet force coefficient, $\frac{\text{isentropic force}}{qS}$

C_{J_I} total isentropic thrust coefficient, $C_{J_A} + C_{\mu_a}$

C_L lift coefficient, $\frac{\text{lift}}{qS}$

$C_{L_{AERO}}$ C_L used for wall corrections (see "Data Reduction")

C_m pitching-moment coefficient, $\frac{\text{pitching moment}}{qSc}$

C_T augmentor turbocompressor jet-pipe thrust coefficient, $\frac{\text{thrust}}{qS}$

C_v thrust (velocity) coefficient (ratio of measured thrust to thrust using measured flow and isentropically expanded jet velocity)

C_{μ_a} isentropic aileron boundary-layer control (BLC) coefficient, $\frac{\text{isentropic BLC force}}{qS}$

h lobe height of primary nozzle, inside dimension see figure 3(g), cm (in.)

ℓ_z distance from face of primary nozzle to flap pivot, see figure 3(b), m (ft)

p primary nozzle lobe spacing, see figure 3(g), cm (in.)

P_a ambient pressure, N/m^2 (in Hg)

P_T wing duct total pressure, N/m^2 (in Hg)

P_{T_N} total pressure at exit of calibrating nozzle, N/m^2 (in Hg)

q free-stream dynamic pressure, N/m^2 (lb/ft^2)

S wing area, sq m (sq ft)

t airfoil thickness, or primary nozzle lobe width inside dimension (fig. 3(g)) m (ft), cm (in.)

x chordwise station, m (ft)

y airfoil ordinate or distance out from the model plane of symmetry, m (ft)

z distance from primary nozzle center and tangent to flap upper surface, see figure 3(b), cm (in.)

Z distance between moment center and line of action of tailpipe thrust, m (ft)

α model angle of attack, deg

δ_a aileron deflection, positive with trailing edge down, deg

δ_f augmentor flap deflection measured with respect to centerline of the diffuser, (see fig. 3(a), deg)

δ_{JP} deflection of augmentor turbocompressor jet pipes relative to fuselage datum plane, deg

δ_s slat deflection, (see fig. 2(c)), deg

η wing station, (distance from model plane of symmetry), 2y/b

ϕ_G ratio of measured augmentor thrust to measured primary nozzle thrust

ϕ_N ratio of measured augmentor or primary nozzle thrust to isentropic nozzle thrust

Subscripts:

a aileron

A augmentor

f flap

JP jet pipe

i isentropic

L left

R right

s slat

u uncorrected for wall effects

uu uncorrected for either wall effects or jet-pipe thrust

MODEL AND APPARATUS

Basic Model

The model is shown installed in the wind tunnel in figures 1(a) and (b). The basic geometric details of the model are summarized in figure 2 and the model reference dimensions and airfoil coordinates are listed in tables 1 and 2. Except for slight modifications to the aileron and L.E. slat, the basic configuration is similiar to that for which test results are reported in references 1, 3 and 4. All tests were made without horizontal tail, underslung engine pods, and fuselage boundary-layer control (BLC).

As with the previous investigations using the model, the air for the augmentor and aileron BLC systems was supplied by a pump consisting of two turbocompressors, or modified viper engines driven by a J-85 turbojet engine. The turbines of the vipers were driven by the J-85 hot gas which was then ejected at the rear of the fuselage through two tailpipes. A diagram of this pumping system is presented in figure 2(e) of reference 4.

The geometry of the aileron and aileron BLC is presented in figure 5 of reference 4, also see figure 2(b) of this report. The system was fed through an extension of the augmentor primary air duct without a valve and therefore, always functioned when the augmentor was operating. Airflow to the aileron was 5% of the total turbocompressor airflow.

Augmentor Flap

The geometry of the flap cross section is shown in figure 3(a). The flap and shroud configuration was the same as that of reference 4 except for the following: (1) the augmentor assembly was reinstalled using the bracket configuration shown in figure 3(b) to facilitate the optimization of augmentor position; (2) the shroud BLC slot inlet lip was rounded and a flexible sealer plate was installed over the intake door hinge as shown in figure 3(c), (note that the intake door was set at its optimum position for each flap angle); and (3) the nozzle configuration had been changed from the slot nozzle of the previous investigation to a lobed configuration. The nozzles, installed, are shown without and with a fiberglass fairing in figures 3(d) and 3(e). Geometric details of the nozzle installation are presented in figures 3(f), 3(g), and 3(h). The configuration shown resulted from the static test program completed by the De Havilland Aircraft of Canada, Limited, using a short-span augmentor, and the static performance improvement measured for the complete model are close to that predicted from results of those tests.

TESTS

A run index of the model configuration and test conditions is presented in table 3. To measure the augmentor thrust at zero airspeed, the tests were made with the mo el at zero attitude with the overhead doors of the test section open. The tests were completed as quickly as possible in order to minimize entrainment of the flow through the test section. The test procedure for the wind on testing consisted primarily of varying angle-of-attack at a given combination of power and airspeed. All tests were made at zero sideslip and at flap and aileron settings which were symmetrical except for run 1. All flap, aileron and leading-edge slat settings were set within ±1/2° of the values listed and the duct pressures listed are within ±1 in Hg of the measured values. The value of C_J listed for each polar in the numerical average of values at all angles of attack.

DATA REDUCTION

For all force and moment data, the effects of compressor residual jet thrust, and the intake momentum drag of the fuselage mounted J-85 and viper compressors have been subtracted from the measured values. The corrections made for thrust and momentum drag are as follows:

$$C_{L_u} = C_{L_{uu}} - C_T \sin(\alpha - \delta_{JP})$$

$$C_{D_u} = C_{D_{uu}} - C_{D_m} + C_T \cos(\alpha - \delta_{JP})$$

$$C_{m_u} = C_{m_{uu}} - C_T \frac{Z}{\bar{c}}$$

The forces and moments are referred to the stability axes. The moment center used for data computation was located longitudinally at $0.25\bar{c}$ and vertically $0.20\bar{c}$ below the wing chord plane.

Initial values of C_{J_I} were computed on the basis of the measured mass flow and total pressure in the wing duct feeding the primary nozzles. To verify the duct calibration, and because the analysis of the previous calibration indicated the measured flow rates to be suspect, the wing ducts were disconnected from the compressor and replaced with the calibrating nozzles shown in figures 4(a) and (b). The calibration run was designated run 70 as indicated in table 3. A detailed analysis of the use of this run is presented in reference 5 but a summary of the results is presented in figure 4(c). The symbol C_d was derived from values of $C_V C_d$ using data from calibrations of the nozzles. Also shown are values of C_d (indicated for the calibrating nozzles using flow rates derived from the viper metering pressures. These were clearly in error and all flow quantities derived for the earlier test runs were corrected downward as indicated.

Wind-tunnel boundary corrections were based upon the lift coefficient evaluated as follows:

$$C_{L_{AERO}} = C_{L_u} - C_{J_A} \sin(\delta_f + \alpha_u) - C_{\mu_a} \sin(\delta_a + \alpha_u)$$

Then the following boundary corrections were made:

$$\alpha = \alpha_u + 0.458\ C_{L_{AERO}}$$

$$C_D = C_{D_u} + 0.00799\ C_{L_{AERO}}^2$$

DATA PRESENTATION

Results of wind off tests are presented in figures 5 and 6. The results of test runs 1 and 69 with the shroud and flap removed were somewhat different, the latter showing higher efficiency. No definite reason for this has been determined, but it is the opinion of the authors that the latter results are more valid since they were obtained after repeated calibration of the data aquisition system and are closer to the unpublished results obtained by the De Havilland Aircraft of Canada. These results are also shown in figure 5 for reference. Both net (ϕ_N) and gross (ϕ_G) augmentation ratios with the complete augmentor installed are also presented in figure 5. Gross augmentation values with the shroud off are presented in figure 6 and are based on the primary nozzle thrust values measured in run 69.

Results of tests at airspeed are presented in figures 7 through 23. Table 4 is an index to the figures. The effect of power on the performance for several augmentor and leading-edge slat configurations are presented in figures 7 through 16. Figure 17 shows the effect of possible metric-nonmetric mechanical interference in the support system which was suspected for some of the later tests. As shown, any effect proved small. Results of additional attempts to repeat test conditions are presented in figure 18. The remaining figures show effects of changing wing-augmentor configurations.

REFERENCES

1. Koenig, David G.; and Falarski, Michael D.: Aerodynamic Characteristics of a Swept Augmentor Wing. NASA TM X-62,252. Paper No. 7, STOL Technology Conference, Ames Research Center, Moffett Field, Calif., October 17-19, NASA SP-320, 1972.

2. Aiken, Thomas N.: Advanced Augmentor-Wing Research. Paper No. 8, STOL Technology Conference, Ames Research Center, Moffett Field, Calif., October 17-19, NASA SP-320, 1972.

3. Falarski, Michael D.; and Koenig, David G.: Longitudinal and Lateral Stability and Control Characteristics of a Large-Scale Model with a Swept Wing and Augmented Jet Flap. NASA TM X-62,145, 1972.

4. Falarski, Michael D.; and Koenig, David G.: Longitudinal Aerodynamic Characteristics of a Large-Scale Model with a Swept Wing and Augmented Jet Flap in Ground Effect. NASA TM X-62,174, October 1972.

5. Garland, D. B.; and Whittley, D. G.: Thrust Performance of a Large-Scale Augmentor-Wing Model, NASA CR-152170, 1978.

TABLE 1.— REFERENCE DIMENSIONS

Wing	
Wing area, sq m (sq ft)	21.36(230.0)
Aspect ratio	8.0
Span, m (ft)	13.08(42.895)
Taper ratio	0.30
Sweep at 1/4 chord deg	27.5
Airfoil section	RAE 104
Root chord, m (ft)	2.515(8.25)
Tip chord, m (ft)	0.755(2.475)
Root thickness, percent	12.5
Tip thickness, percent	10.5
Augmentor span limits, inner, m (ft) (percent)	1.111(3.645)(12.34)
Augmentor span limits, outer, m (ft) (percent)	4.575(15.01)(70.0)
Wing area spanned by one augmentor, sq m (sq ft)	6.75(72.62)
Wing area spanned by one aileron, sq m (sq ft)	1.997(21.50)
Wing area spanned by fuselage, sq m (sq ft)	3.88(41.77)
Flap hinge axis, percent chord	68.543
Aileron hinge axis, percent chord	68.0
Incidence, camber, twist	0
Mean aerodynamic chord, m (ft)	1.793(5.880)
Vertical Tail	
Fin arm, m (ft)	5.361(17.603)
Fin volume coefficient	0.07476

Note: All chords are measured in streamwise direction.

TABLE 2.— COORDINATES OF RAE 104 AIRFOIL (t/c max = 0.10)

x/c	y/c(100)	x/c	y/c(100)
0	0	0.35	4.9300
0.001	0.3441	.35	4.9488
.002	.4863	.38	4.9775
.003	.5953	.4	4.9946
.004	.6870	.42	5.0000
.005	.7676	.44	4.9937
.006	.8404	.45	4.9862
.007	.9072	.46	4.9756
.0075	.9387	.48	4.9454
.008	.9692	.5	4.9027
.009	1.0274	.52	4.8468
.01	1.0824	.54	4.7769
.012	1.1842	.55	4.7363
.0125	1.2083	.56	4.6917
.014	1.2776	.58	4.5802
.016	1.3642	.6	4.4650
.018	1.4452	.62	4.3113
.02	1.5215	.64	4.1370
.025	1.6960	.65	4.0438
.03	1.8522	.66	3.9473
.035	1.9945	.68	3.7452
.04	2.1256	.7	3.5331
.05	2.3617	.72	3.3128
.06	2.5709	.74	3.0861
.07	2.7592	.75	2.9708
.075	2.8468	.76	2.8545
.08	2.9307	.78	2.6103
.09	3.0881	.8	2.3819
.1	3.2336	.82	2.1437
.12	3.4945	.84	1.9055
.14	3.7222	.85	1.7864
.15	3.8254	.86	1.6673
.16	3.9224	.88	1.4202
.18	4.0992	.9	1.1910
.2	4.2556	.92	.9528
.22	4.3936	.925	.8932
.24	4.5149	.94	.7146
.25	4.5697	.95	.5955
.26	4.6208	.96	.4764
.28	4.7124	.975	.2977
.3	4.7905	.98	.2382
.32	4.8556	.9875	.1489
.34	4.9082	1.0	0

TABLE 3.— RUN INDEX FOR 40- BY 80-FOOT WIND-TUNNEL TEST NUMBER 487

Run	δ_f	δ_a	δ_S	δ_{ID}	C_J	P_T		q	
						cm Hg	in Hg	N/m²	lb/ft²
1[a]	OFF	-0.8/+8.3[b]	63	OFF		23 - 69	9 - 27	0	0
2	30	30		30		23 - 24	9 - 28	0	0
3					0.19	28	11	747	15.6
4					.26	66	26	1187	24.8
5					.39			766	16
6					.39			766	16
7					.26			1187	24.8
8					.78			378	7.9
9					.73			383	8
10					1.24			239	5
11					1.49			201	4.2
12					.57			526	11
13					0	0	0	766	16
14			OFF		.19	28	11	747	15.6
15			OFF		.77	66	26	383	8
16			OFF		0	0	0	761	15.9
17			30		.78	66	26	383	8
18					.19	28	11	747	15.6
19					0	0	0	766	16
20					.39	65	26	761	15.9
21					.79			378	7.9
22					1.07			277	5.8
23					1.45			201	4.2
24	15	15		22		23 - 66	9 - 26	0	0
25					.19	28	11	747	15.5
26					.26	66	26	1187	24.8
27					.39			761	15.9
28					.78			383	8
29					1.05			277	5.8
30					1.47			201	4.2
31					0	0	0	766	16
32			OFF		1.46	66	26	201	4.2
33					1.06	66	26	272	5.7
34					.77	66	26	383	8
35					0	0	0	766	16
36		0			1.45	66	26	201	4.2
37		15		Shroud off		23 - 69	9 - 27	0	0
38					1.43	66	26	205	4.3
39					.77	66	26	383	8
40					0	0	0	766	16
41			30		1.46	66	26	201	4.2

[a]Augmentor shroud, off.
[b]Left/right aileron.

TABLE 3.— CONCLUDED

Run	δ_f	δ_a	δ_S	δ_{ID}	C_J	P_T cm Hg	P_T in Hg	q N/m^2	q lb/ft^2
42	15	15	30	Shroud off	1.05	66	26	277	5.8
43					.78			383	8
44					.39			761	15.9
45					.24			1240	25.6
46					.18	28	11	747	15.6
47					0	0	0	766	16
48					--	28 - 69	11 - 27	0	0
49					1.46	66	26	201	4.2
50					1.05			277	5.8
51					.77			383	8
52					.39			766	16
53					.25			1192	24.9
54					.19	28	11	747	15.6
55					0	0	0	766	16
56	30	30			--	23 - 69	9 - 27	0	0
57					1.49	66	26	201	4.2
58					1.06			272	5.7
59					1.47			201	4.2
60					1.05			282	5.9
61					.77			383	8
62					.39			766	16
63					.25			1192	24.9
64					0	0	0	766	16
65					--	23 - 66	9 - 26	0	0
66					--	23 - 66	9 - 26	0	0
67					1.46	66	26	201	4.2
68					.77	66	26	383	8
69	Off	15			--	23 - 69	9 - 27	0	0
70	Supply air calibration				--	23 - 69	9 - 27	0	0

TABLE 4.— INDEX TO DATA PRESENTATION

Figure	Effect	Shroud	Lower slot	δ_f	δ_a	δ_s	C_J Nominal
7	C_J			30	30	60	
8	↓			30	30	Off	
9				30	30	30	
10				15	15	30	
11				↓	↓	Off	
12		Off				Off	
13		↓				30	
14			Sealed			↓	
15			↓	30	30		
16				↓	↓		
17	Fouling, C_J						
18(a)	Repeating conditions						0.8
(b)	Repeating conditions					60	0.25, 0.4, 0.8
19(a)	Slat					Off,30 60	0.2
(b)	Slat					60	0.8
(c)	Slat			15	15	Off,30	0.8, 1.5
20(a)	Flap aileron			15,30	15,30	30	0, 0.2
(b)	Flap aileron			15,30	15,30	30	0.8, 1.5
21	Aileron			15	0,15	Off	1.5
22(a)	Shroud			15	15	30	0
(b)	Shroud			15	15	↓	0.25, 0.8, 1.5
(c)	Shroud			30	30		0.8, 1.5
23(a)	Slot seal			15	15		0, 0.25
(b)	Slot seal			15	15		0.8, 1.5
(c)	Slot seal	↓	↓	30	30	↓	

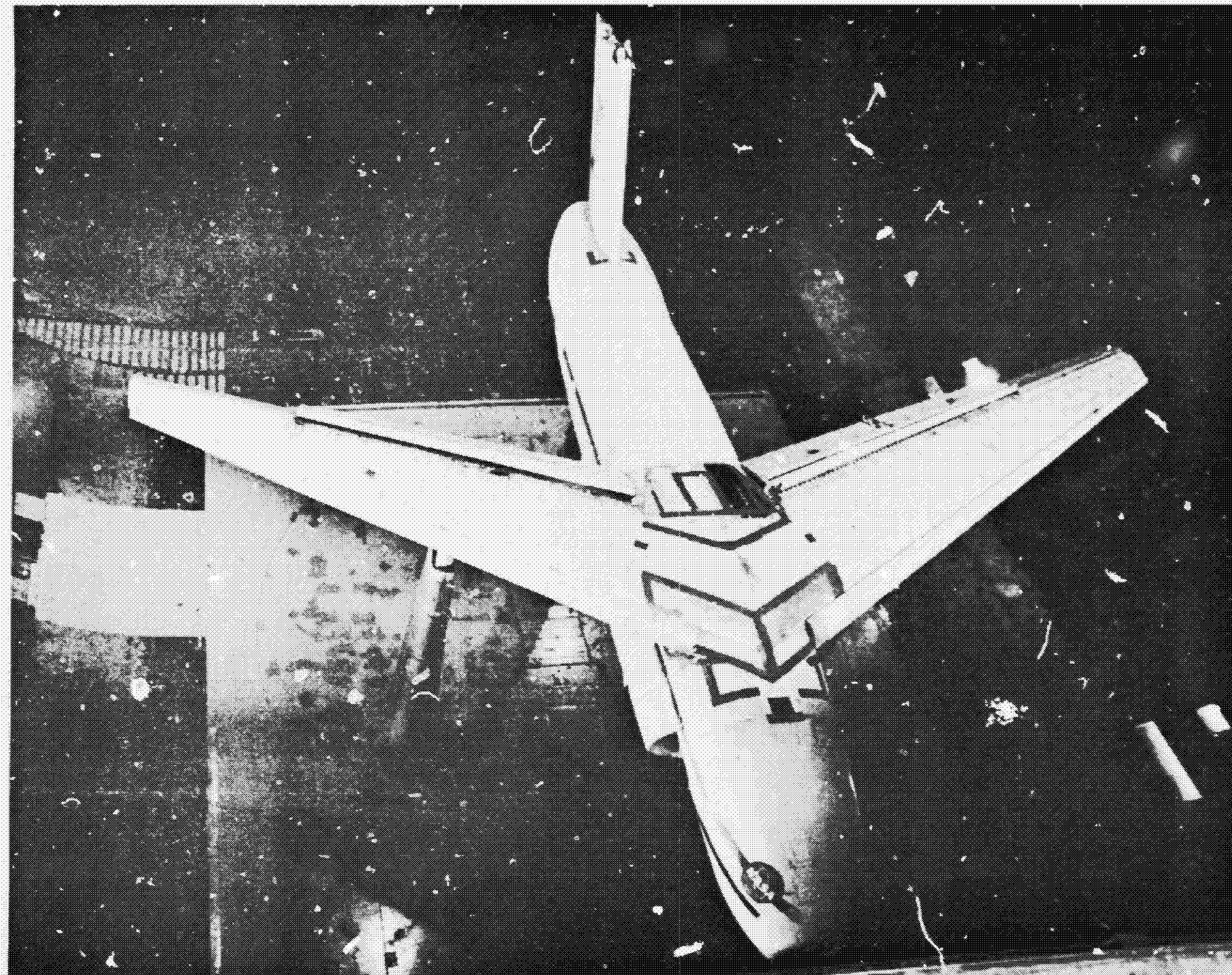

(a) Top view.

Figure 1.– Photograph of the model installed in the Ames 40- by 80-Foot Wind Tunnel.

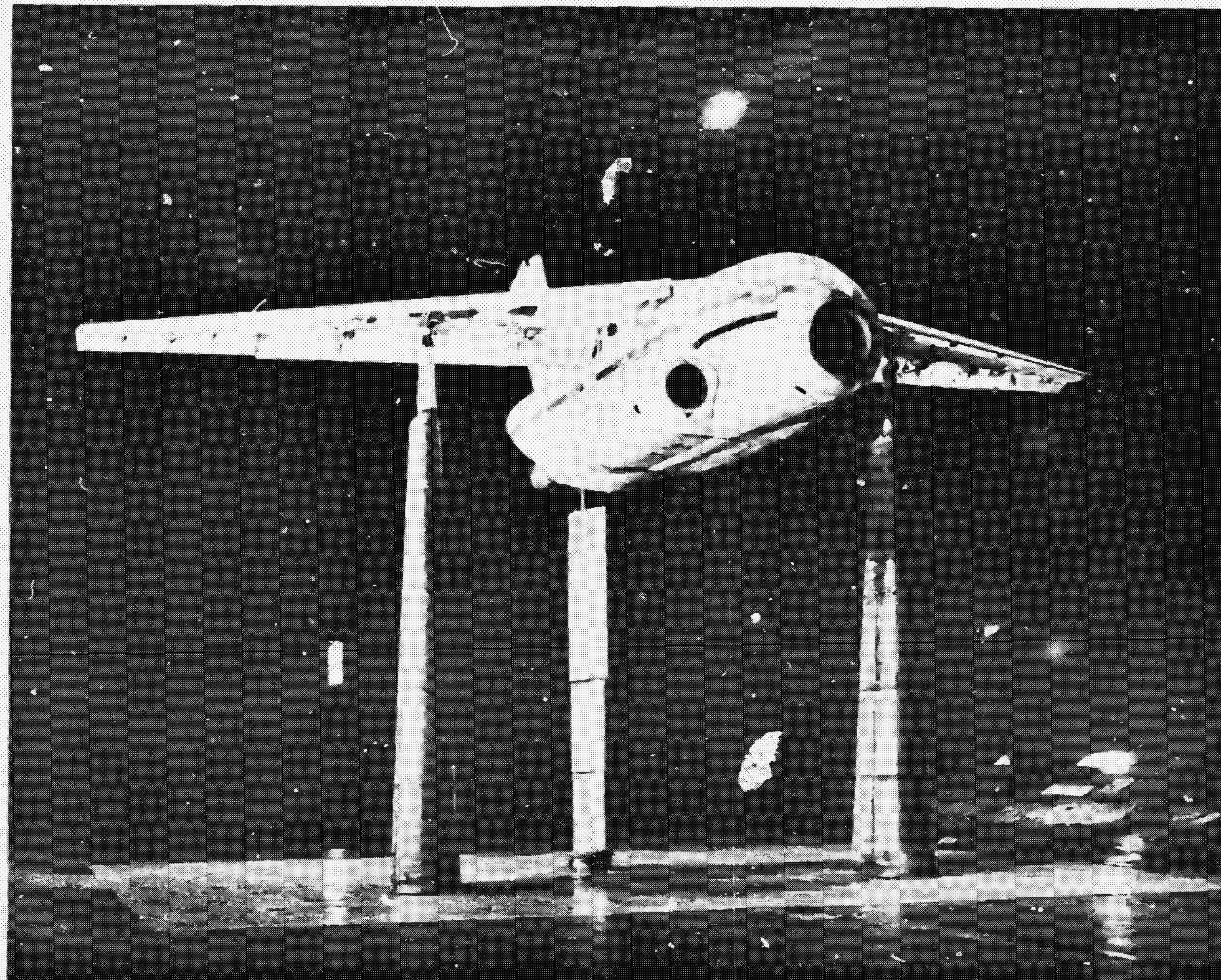

(b) Three-quarter front view.

Figure 1.— Concluded.

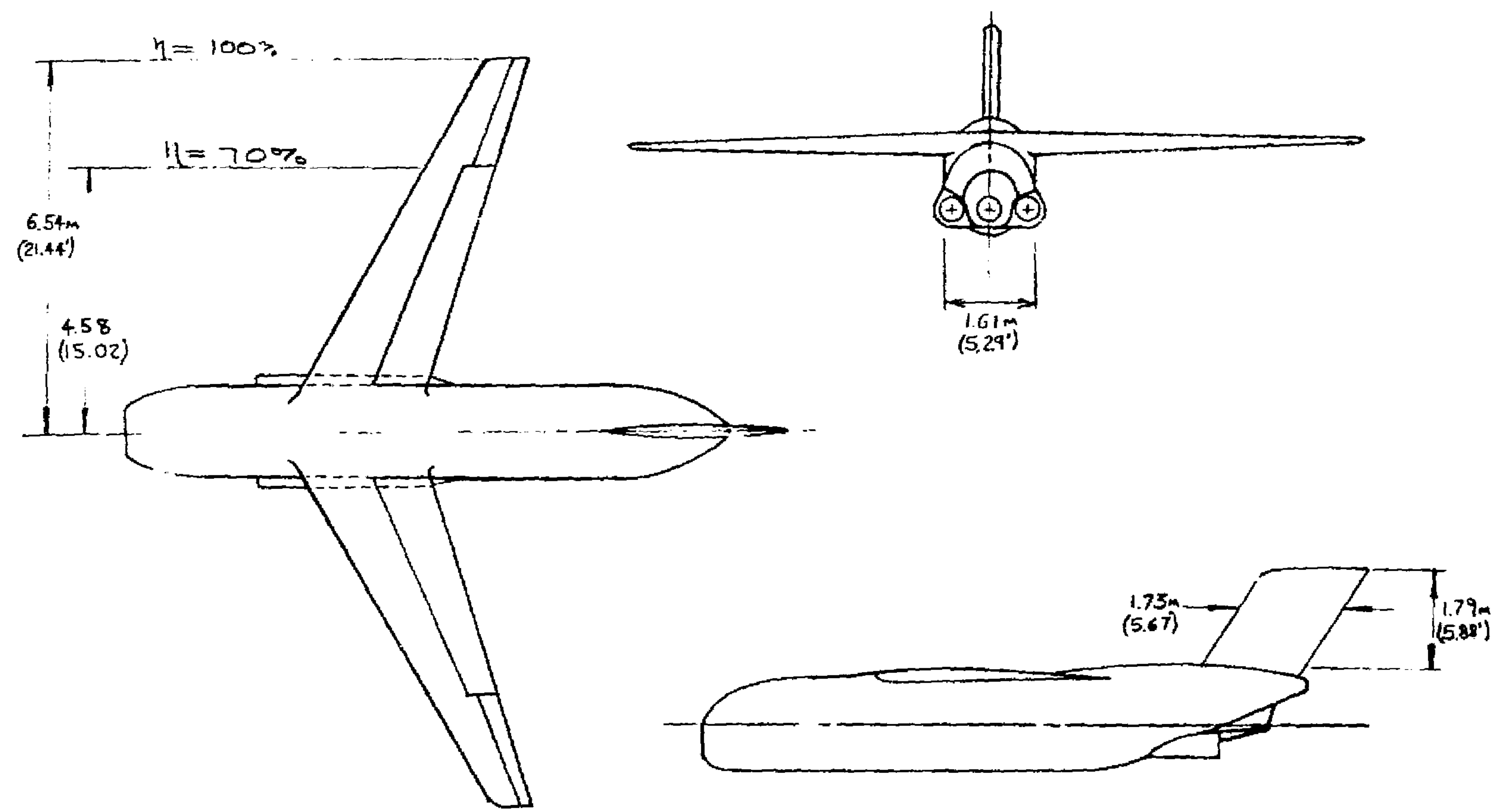

(a) General arrangement.

Figure 2.– Geometric details of basic model.

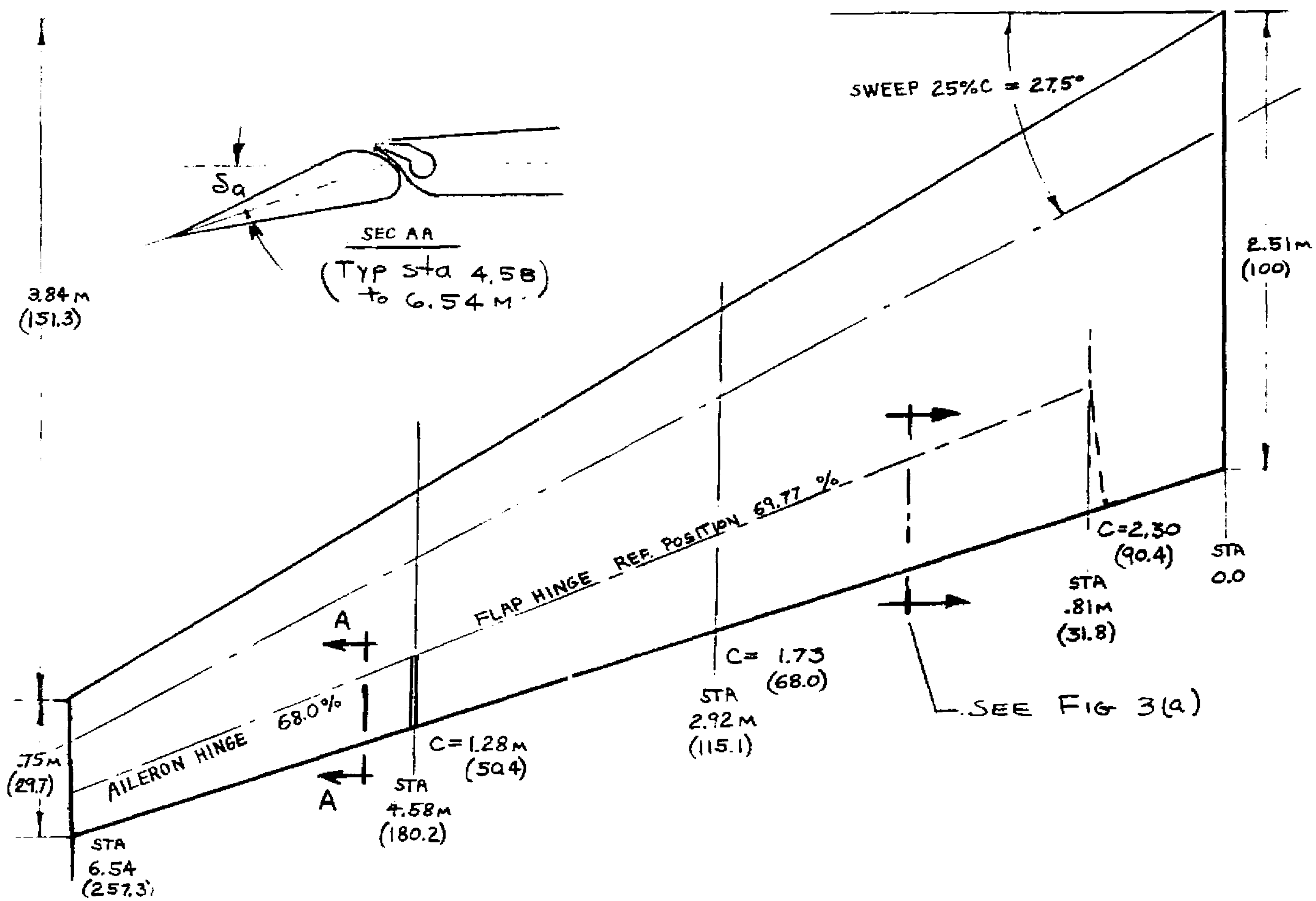

(b) Wing planform.

Figure 2.— Continued.

SLAT CO-ORDINATES	
x/c_s	y/c_s Upper
0.025	0.0667
0.05	0.1000
0.10	0.1520
0.15	0.1843
0.20	0.2088
0.25	0.2255
0.30	0.2375
0.40	0.2500
0.50	0.2476
0.60	0.2265
0.70	0.1941
0.80	0.1431
0.90	0.0794
1.00	0.0000
L.E. RADIUS = 9.314% c_s	

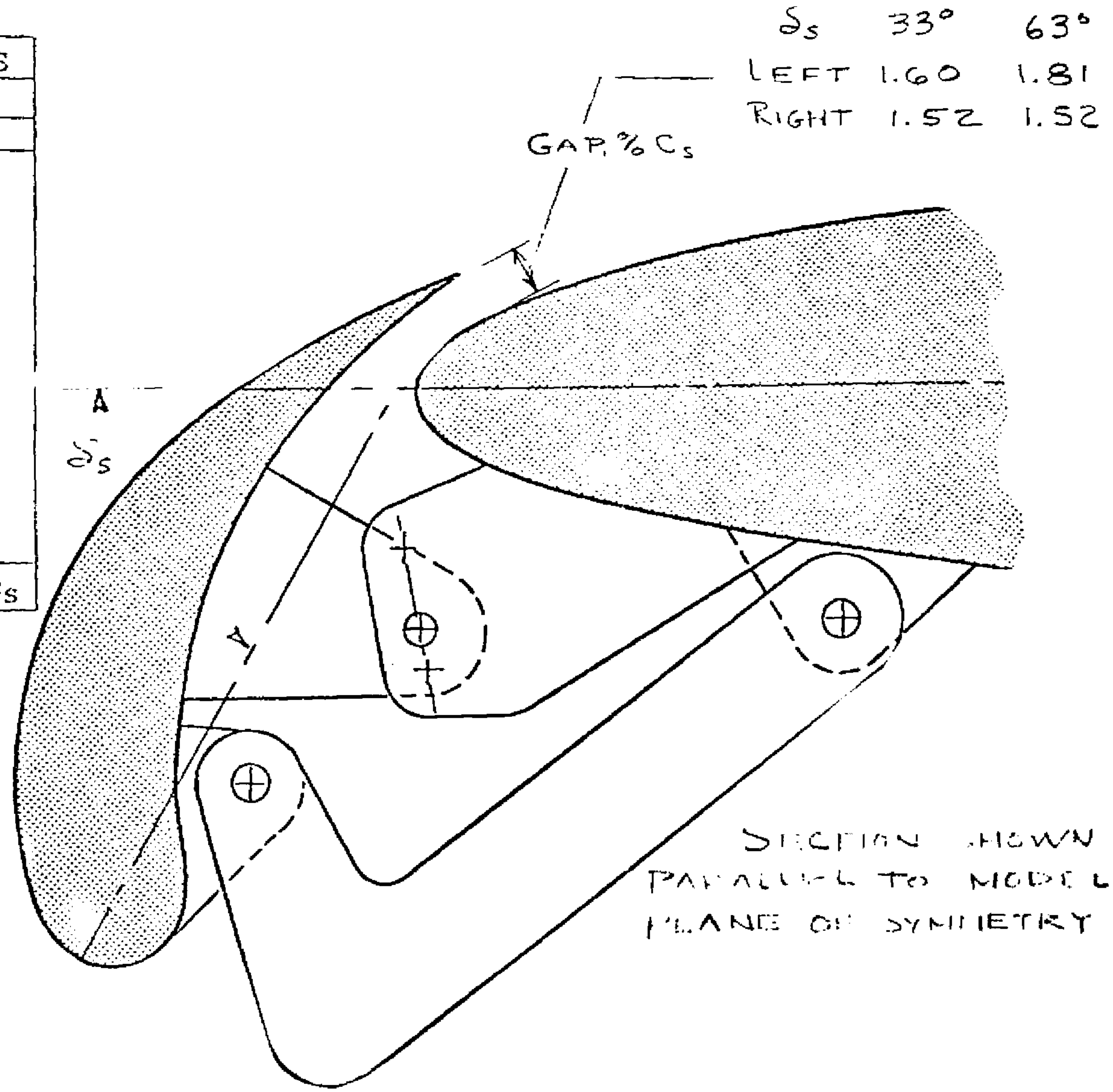

(c) Wing leading-edge slot.

Figure 2.– Concluded.

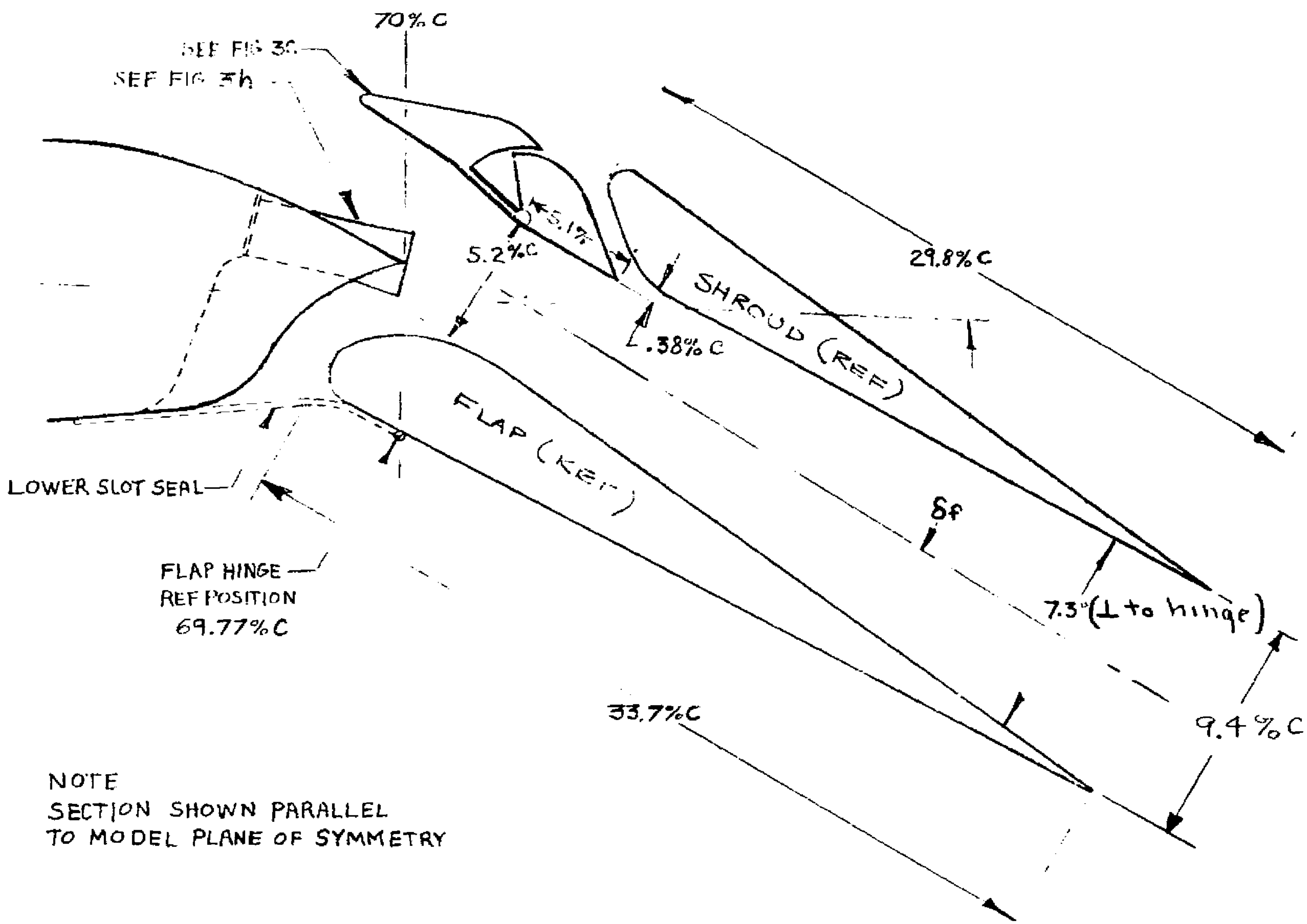

(a) Assembly.

Figure 3.– Details of the thrust augmentor.

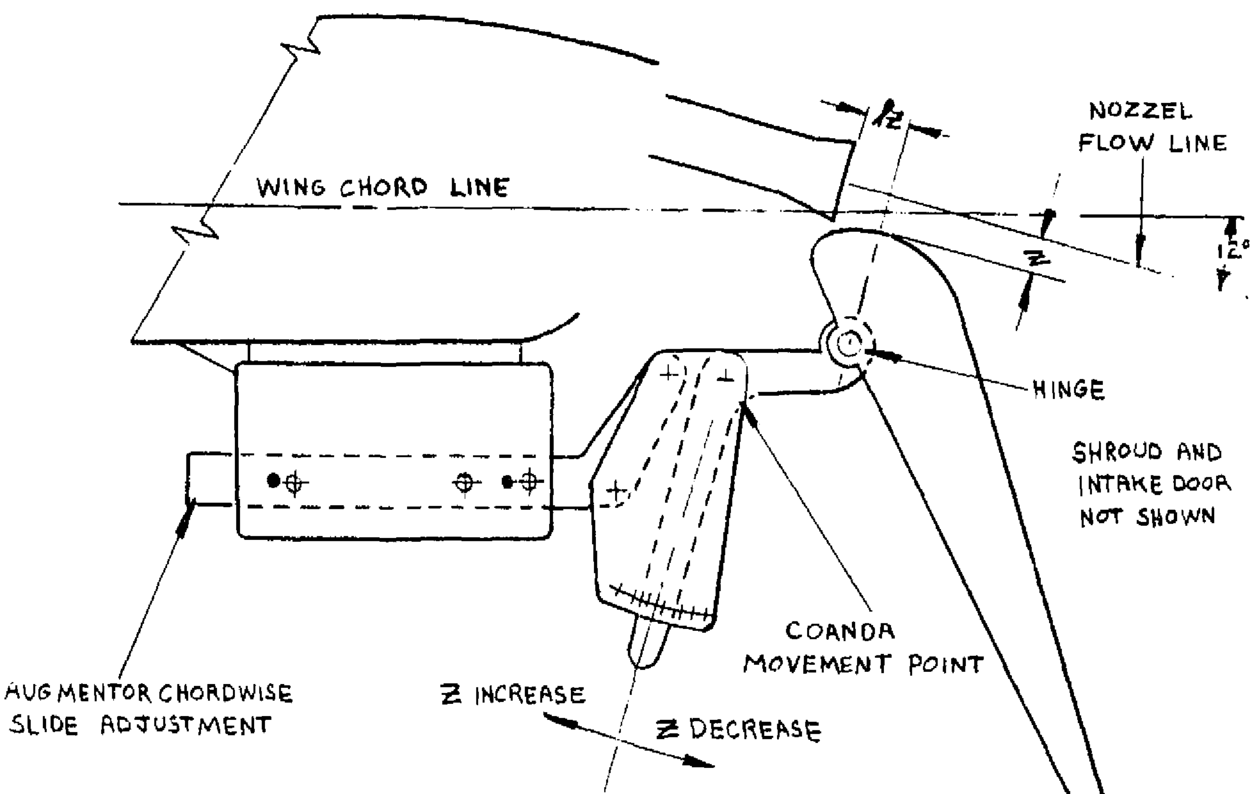

	L	R	L	R
δ_f	15°	15°	30°	30°
z	4.29 cm (1.69)	4.47 cm (1.76)	3.91 cm 1.54	3.68 cm (1.45)
l_z	5.82 cm (2.29)	5.44 (2.14)	4.37 (1.72)	4.27 (1.68)

NOTE:-MEASUREMENTS SHOWN - STREAMWISE,
-ADJUSTMENT MECHANISM, STREAMWISE

(b) Augmentor flap adjustment arrangement.

Figure 3.– Continued.

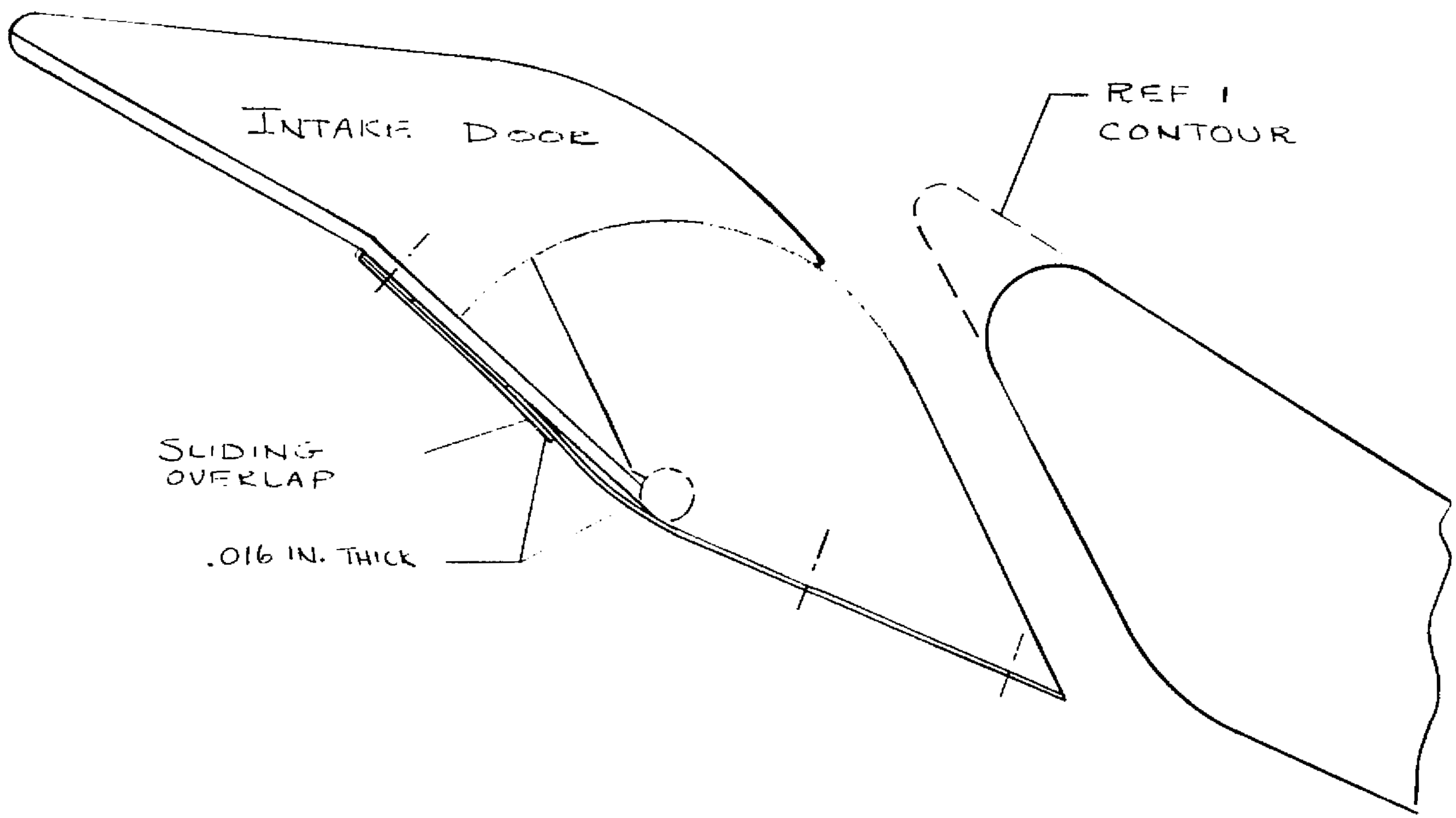

(c) Shroud leading-edge intake door.

Figure 3.-- Continued.

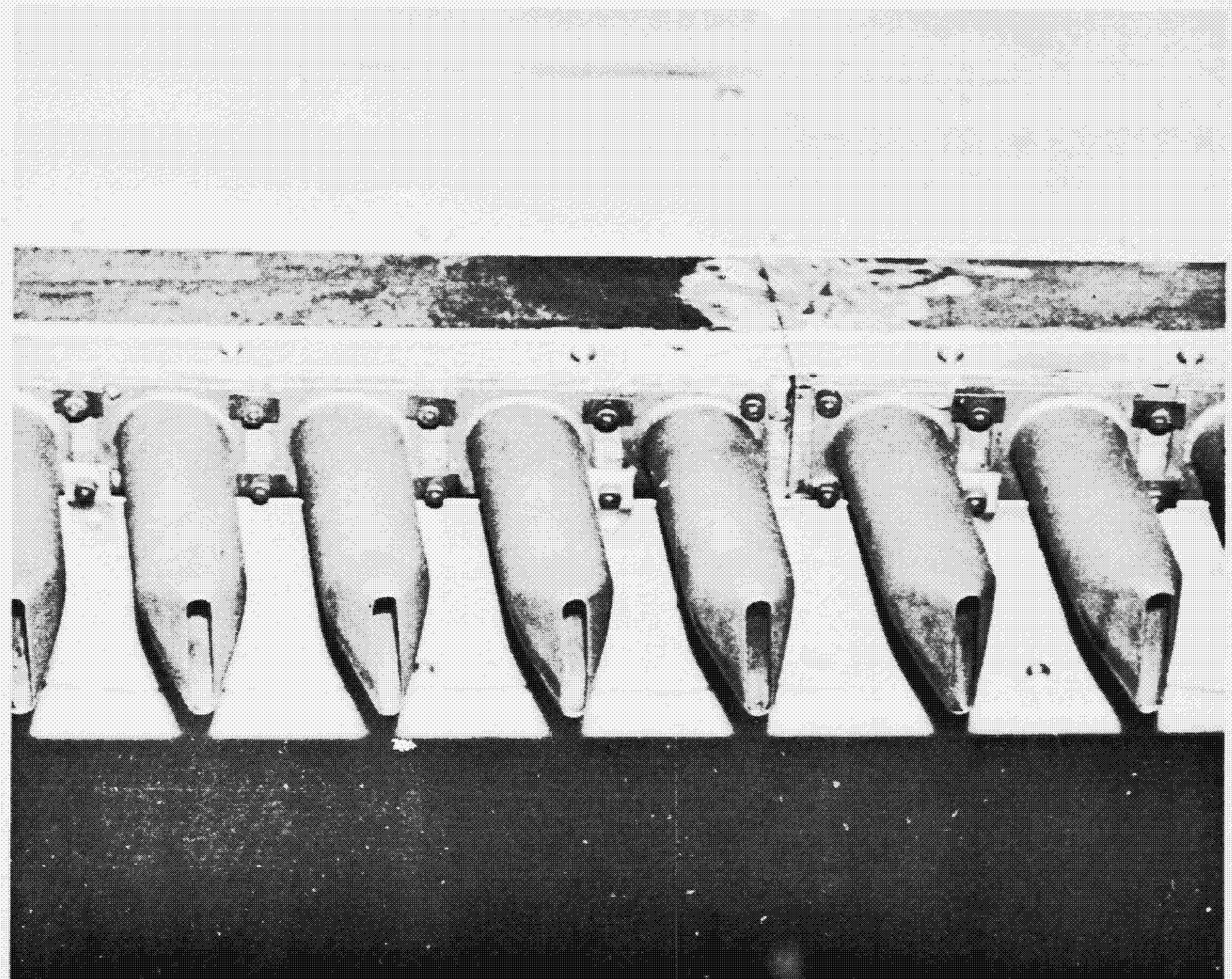

(d) Unfaired nozzles.

Figure 3.— Continued

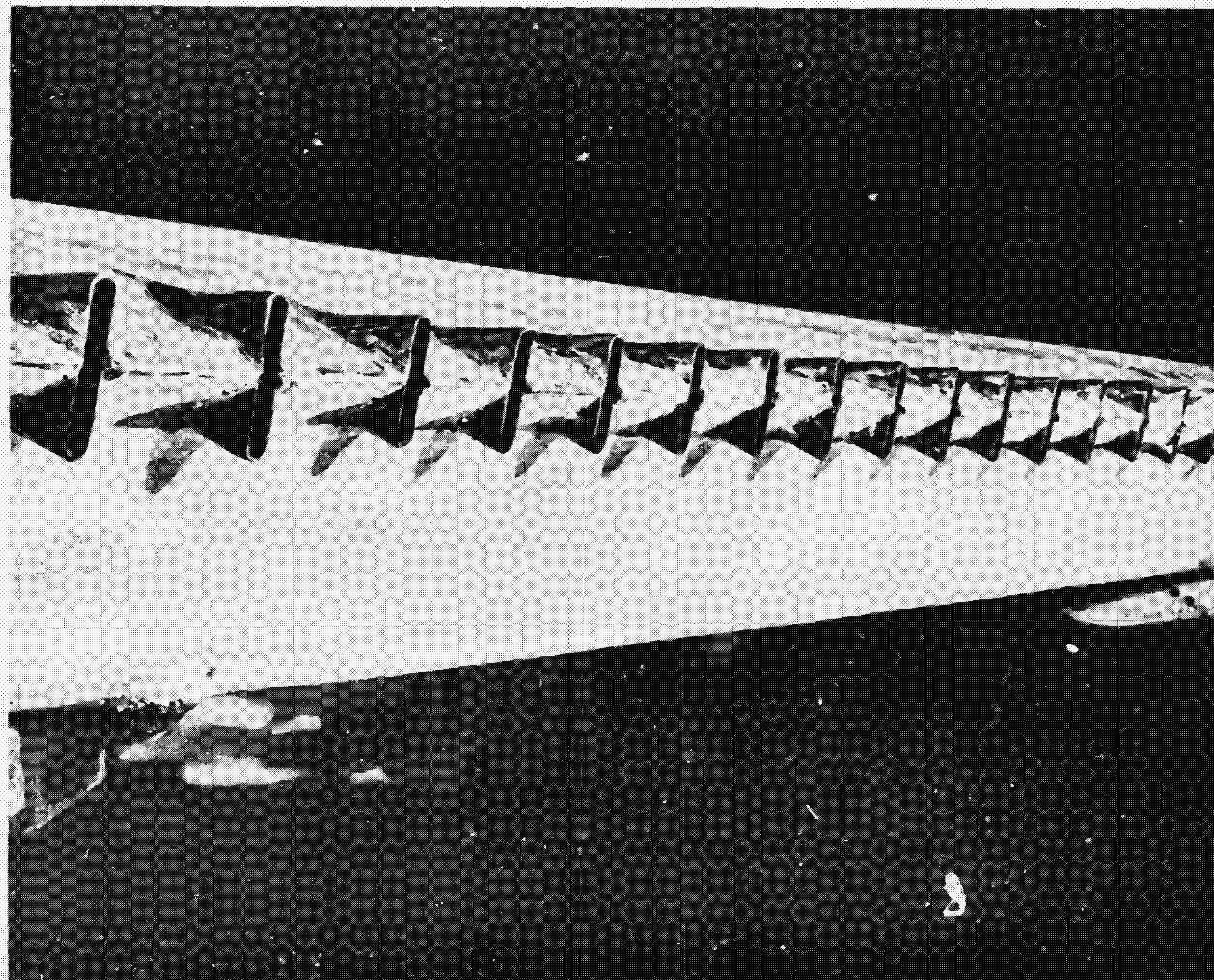

(e) Faired nozzles.

Figure 3.— Continued.

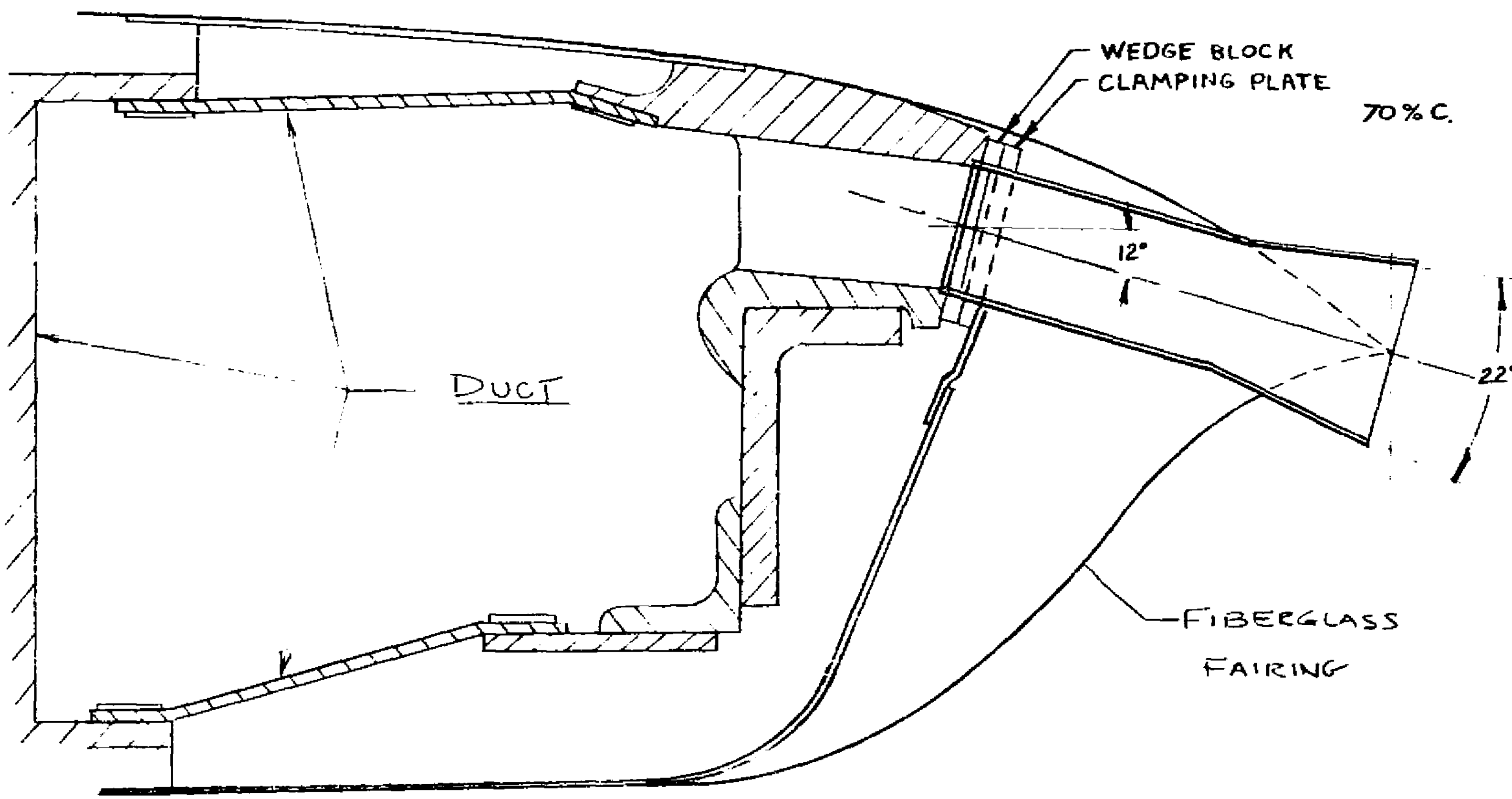

(f) Nozzle-duct arrangement.

Figure 3.— Continued.

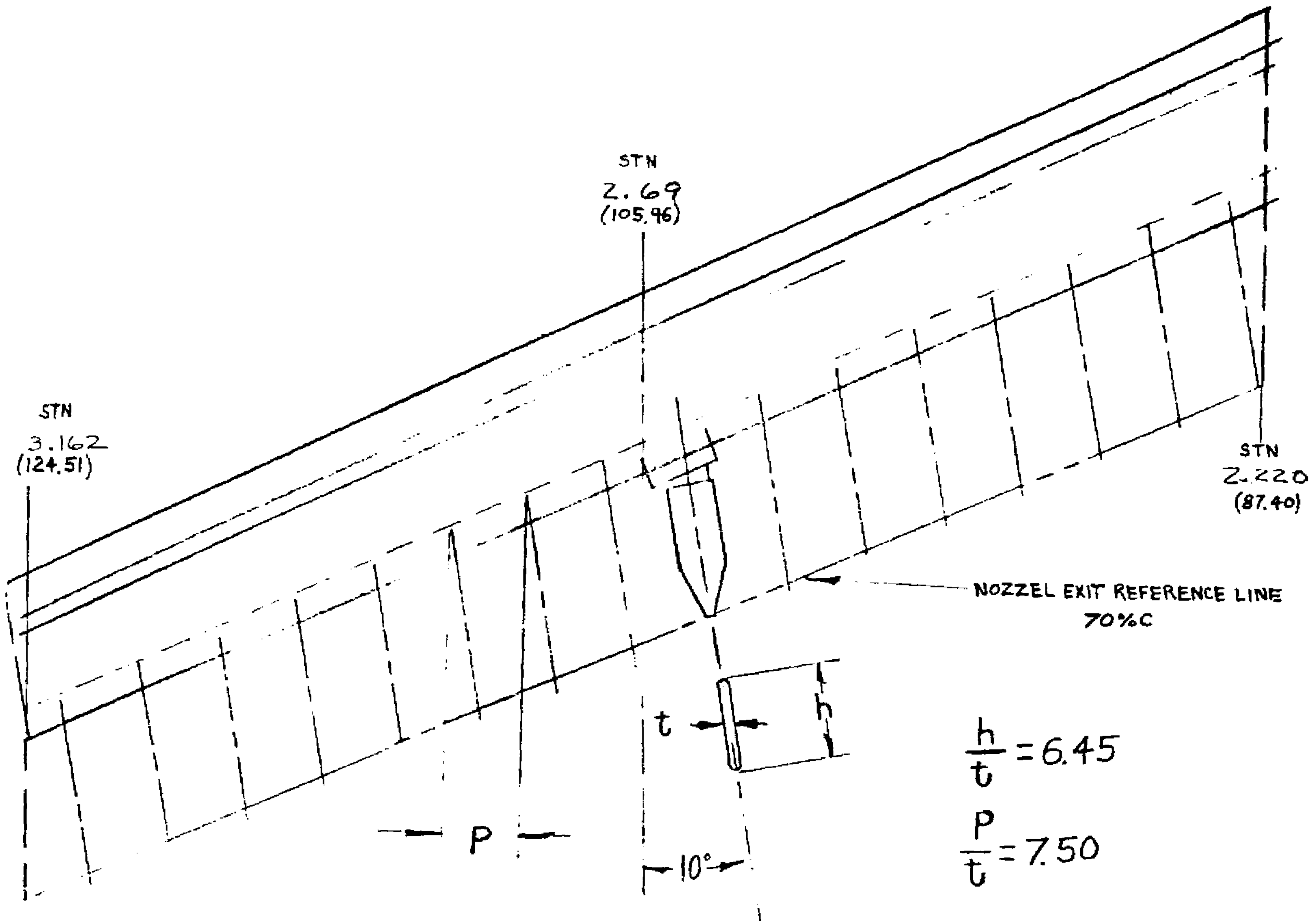

(g) Nozzle-exit geometry and spacing.

Figure 3.— Continued.

NUMBER OF NOZZLES	22	18	16	14
NOZZLE AREA				
TOTAL	46.83 cm² (7.25) IN²	55.17 (8.55)	63.48 (9.84)	71.66 (11.11)
PER LOBE	2.13 cm² (.330) IN²	3.06 (.475)	3.97 (.615)	5.12 (.793)
PITCH P (SPANWISE)	4.28 cm (1.69) IN	5.23 (2.06)	5.89 (2.32)	6.73 (2.65)
INLET DIAMETER	2.74 cm (1.08) IN	3.24 (1.28)	3.56 cm (1.40)	4.20 cm (1.65)

WING CHORD (REF)	1.282 M (50.5) IN.	1.532 (60.3)	1.815 (71.5)	2.043 (80.5)	2.297 (90.4)
SPANWISE STATION	4.576 M 180.2 IN.	3.634 143.1	2.691 106	1.748 68.9	806 (31.8)

(h) Spanwise change in nozzle geometry.

Figure 3.— Concluded.

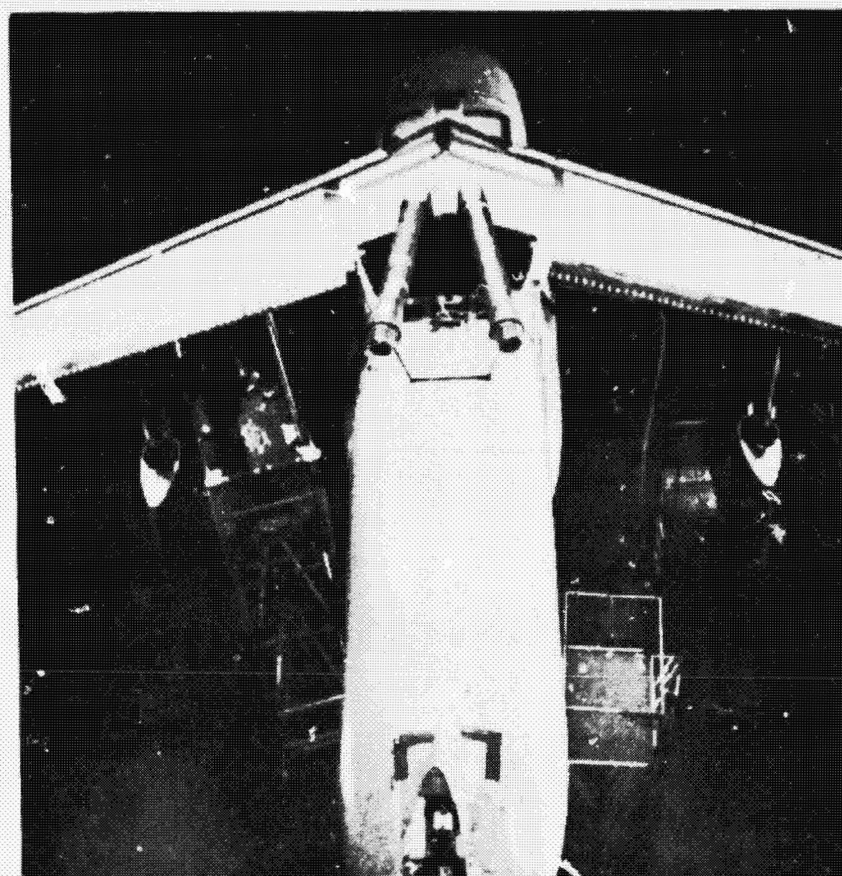

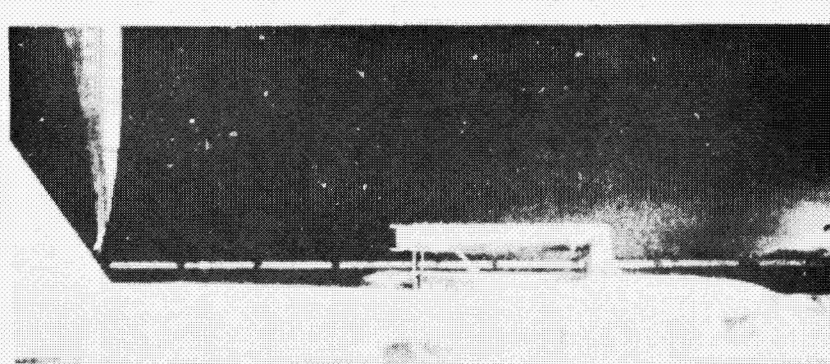

(a) Photograph of installation.

Figure 4.– Calibration nozzle installation.

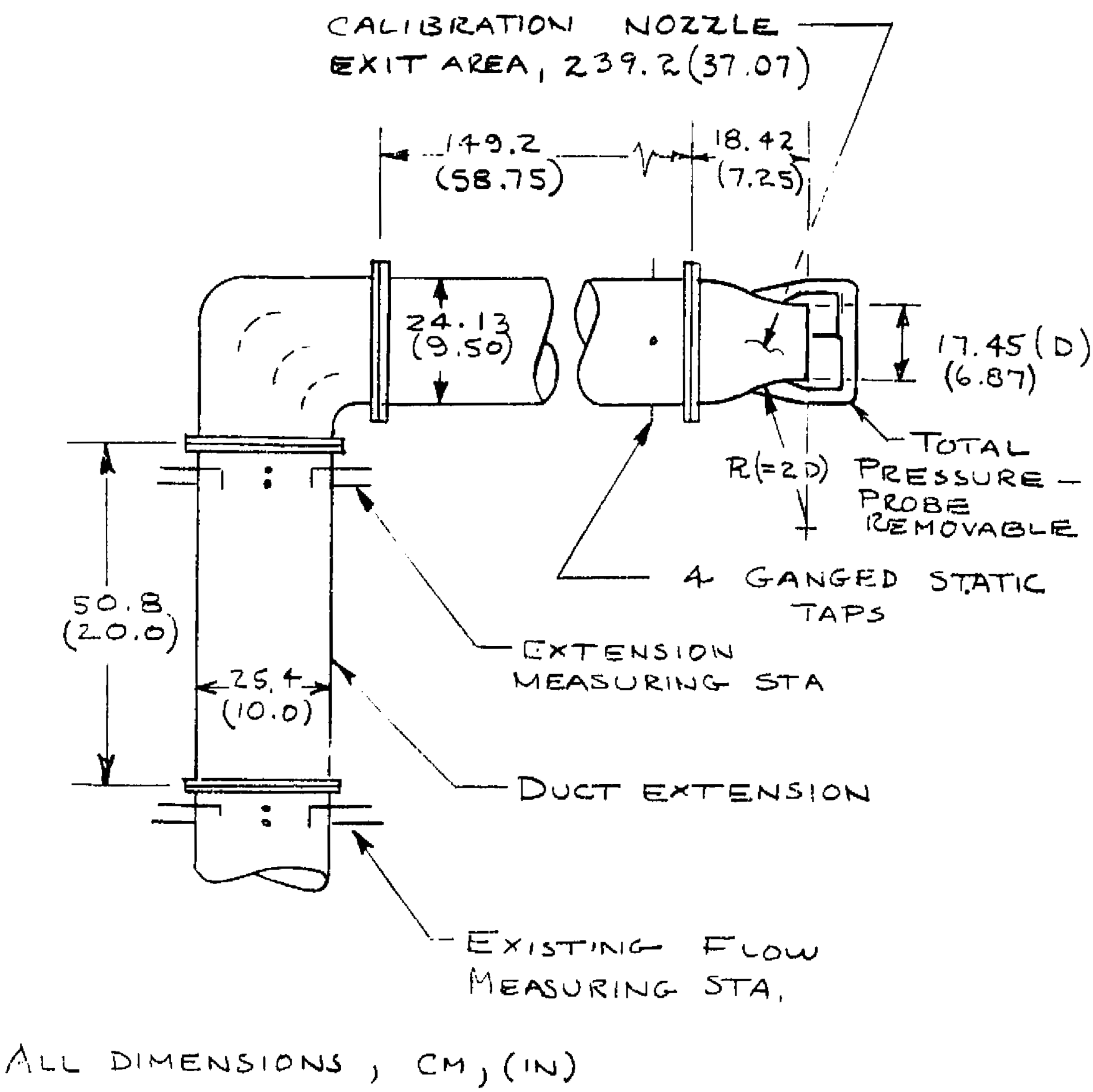

(b) Geometry of nozzle and duct.

Figure 4.— Continued.

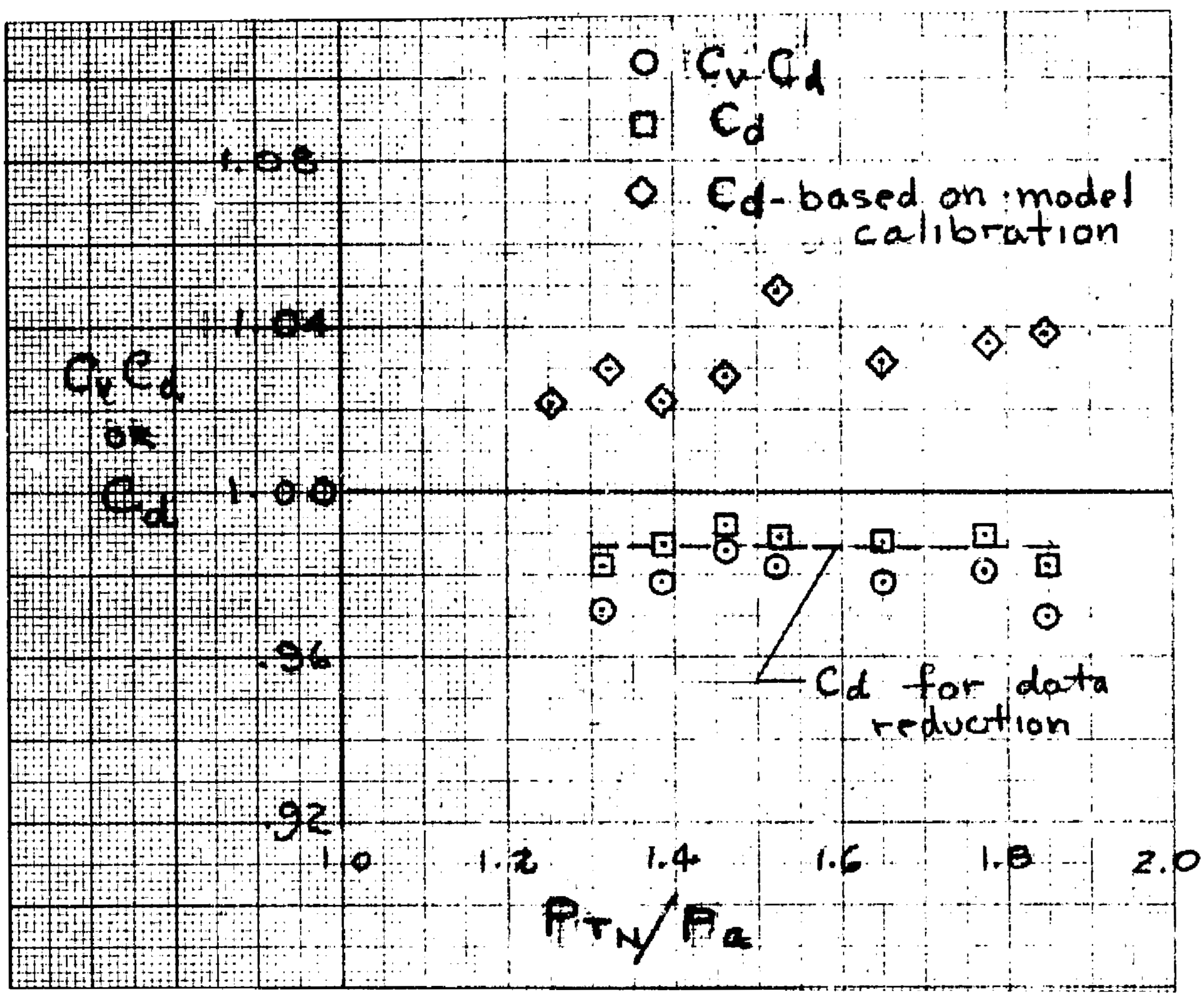

(c) Performance of calibration nozzle.

Figure 4.— Concluded

ORIGINAL PAGE IS
OF POOR QUALITY

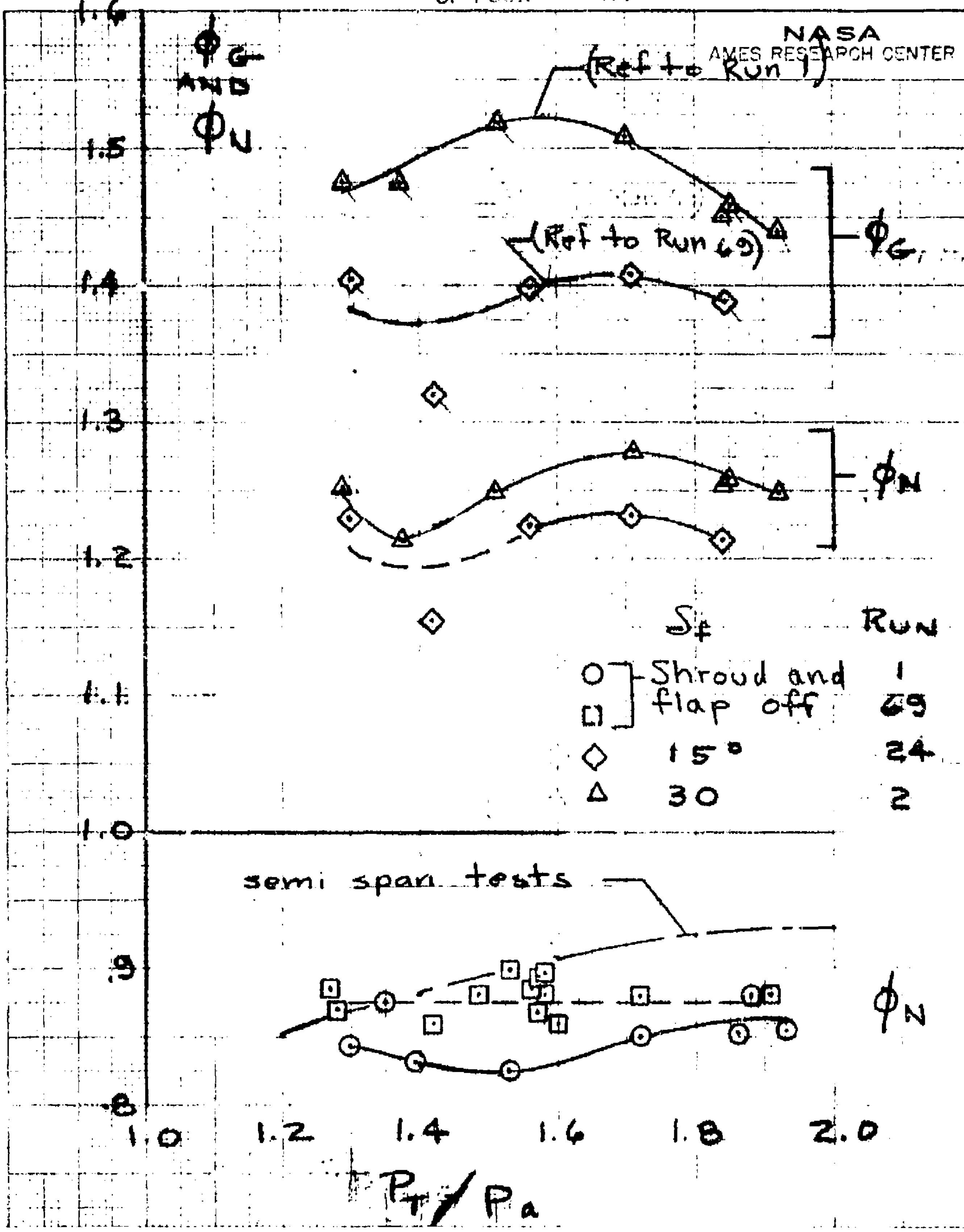

Figure 5.— Static performance with and without augmentor flap and shroud.

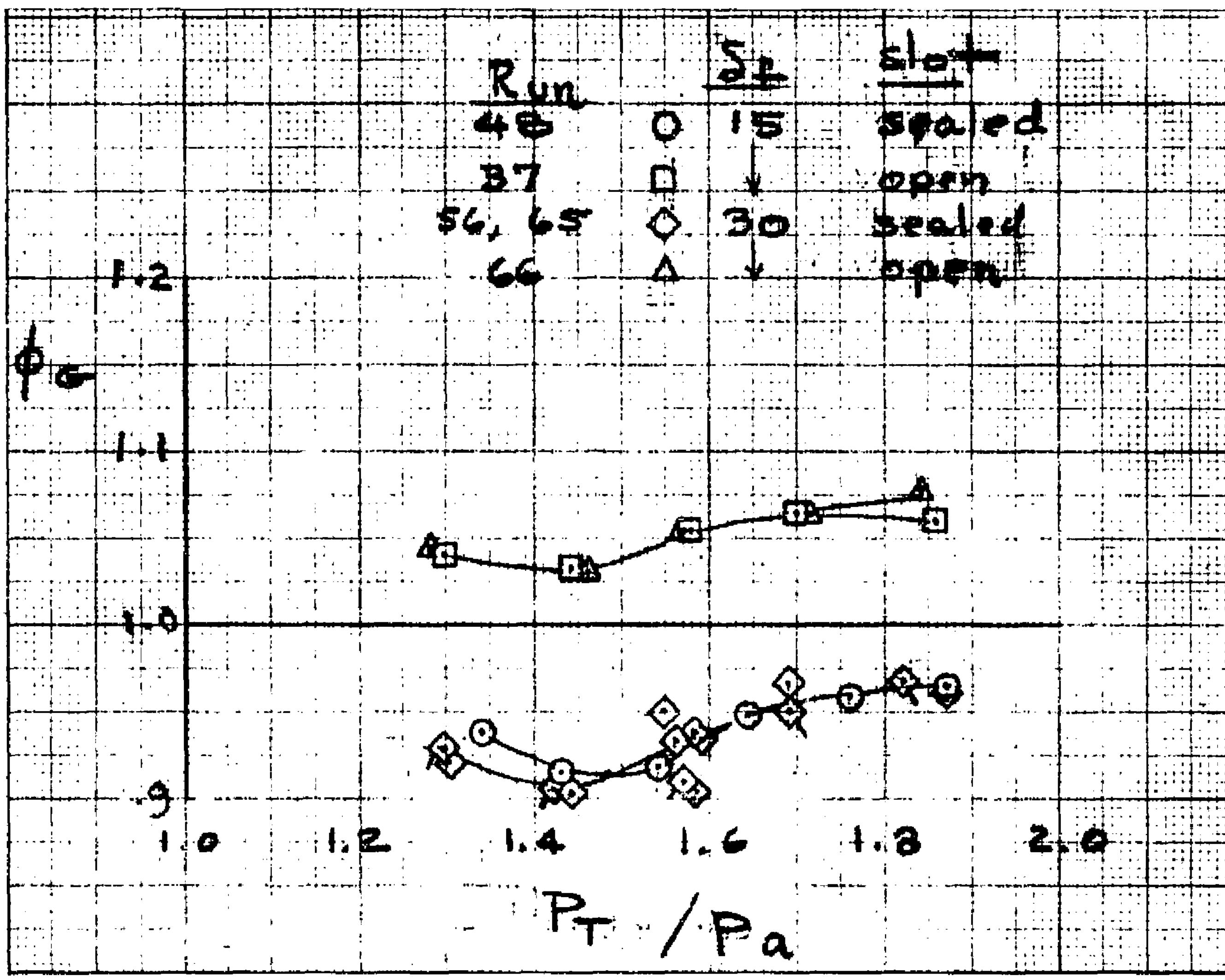

Figure 6.— Effect of sealing lower slot on static performance with shroud off

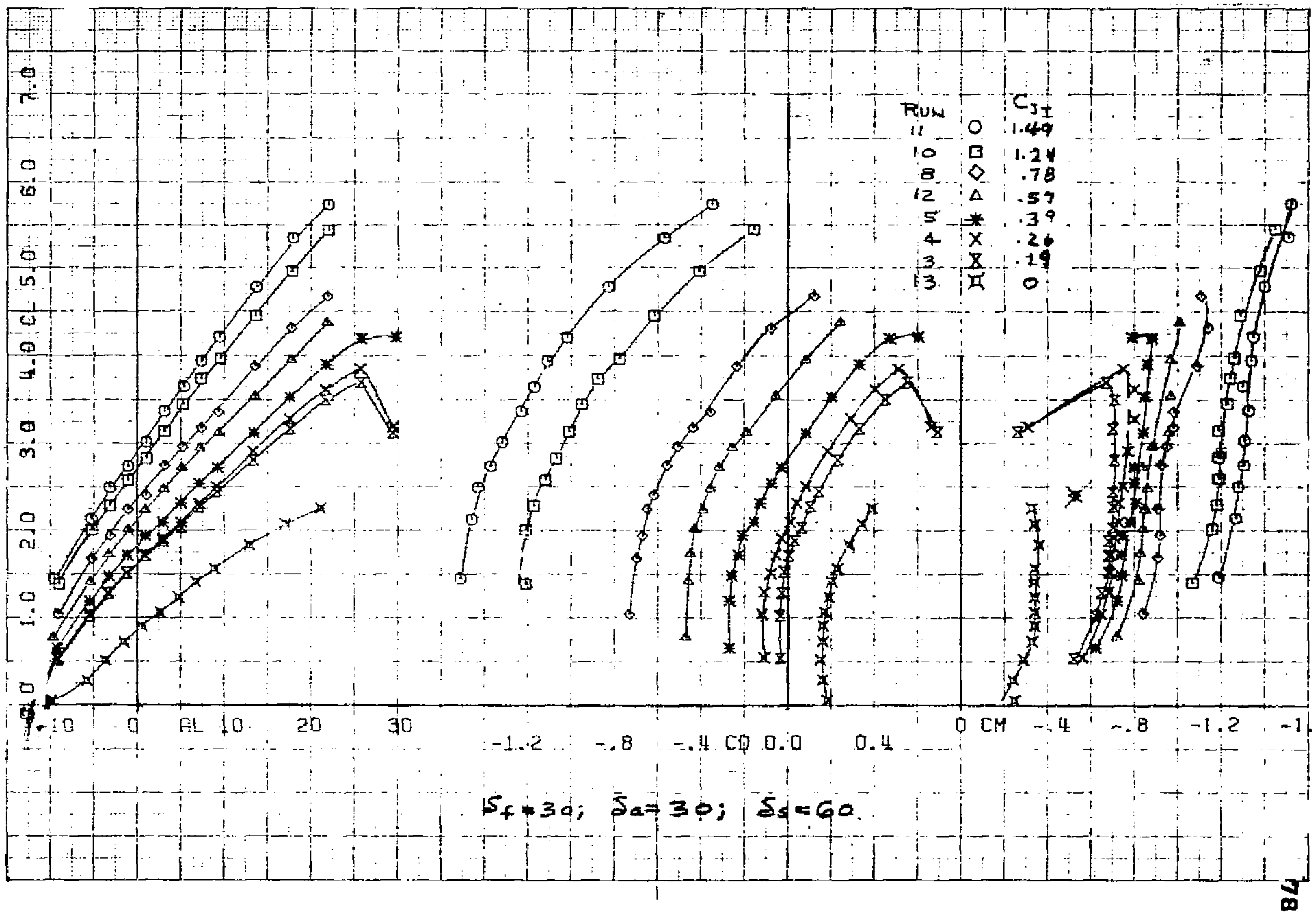

Figure 7.- Characteristics with the shroud and leading-edge slat on; δ_f and δ_a, 30°; δ_s, 60°.

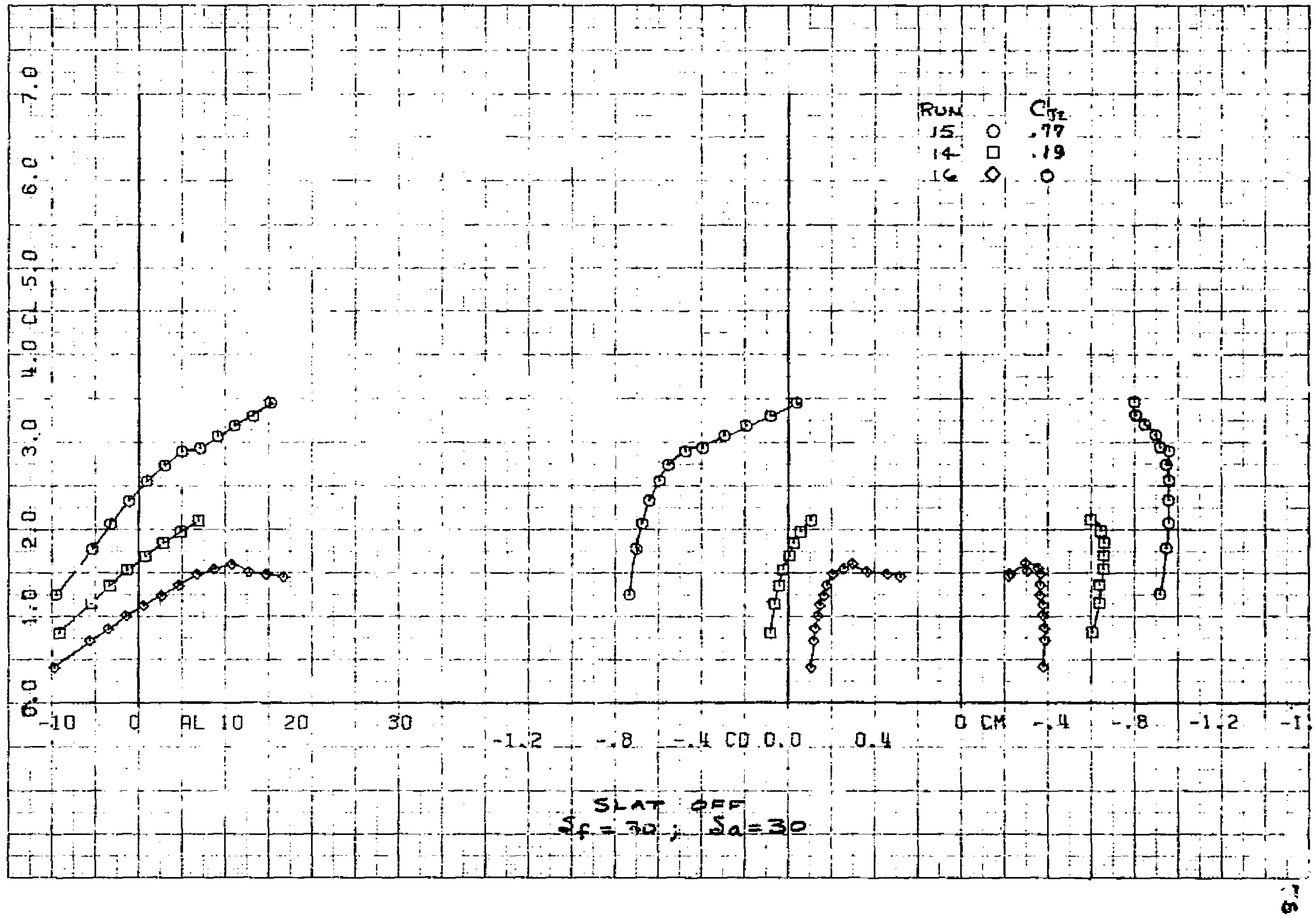

Figure 8.- Characteristics with the shroud on and leading-edge slat off; δ_f and δ_a, 30°.

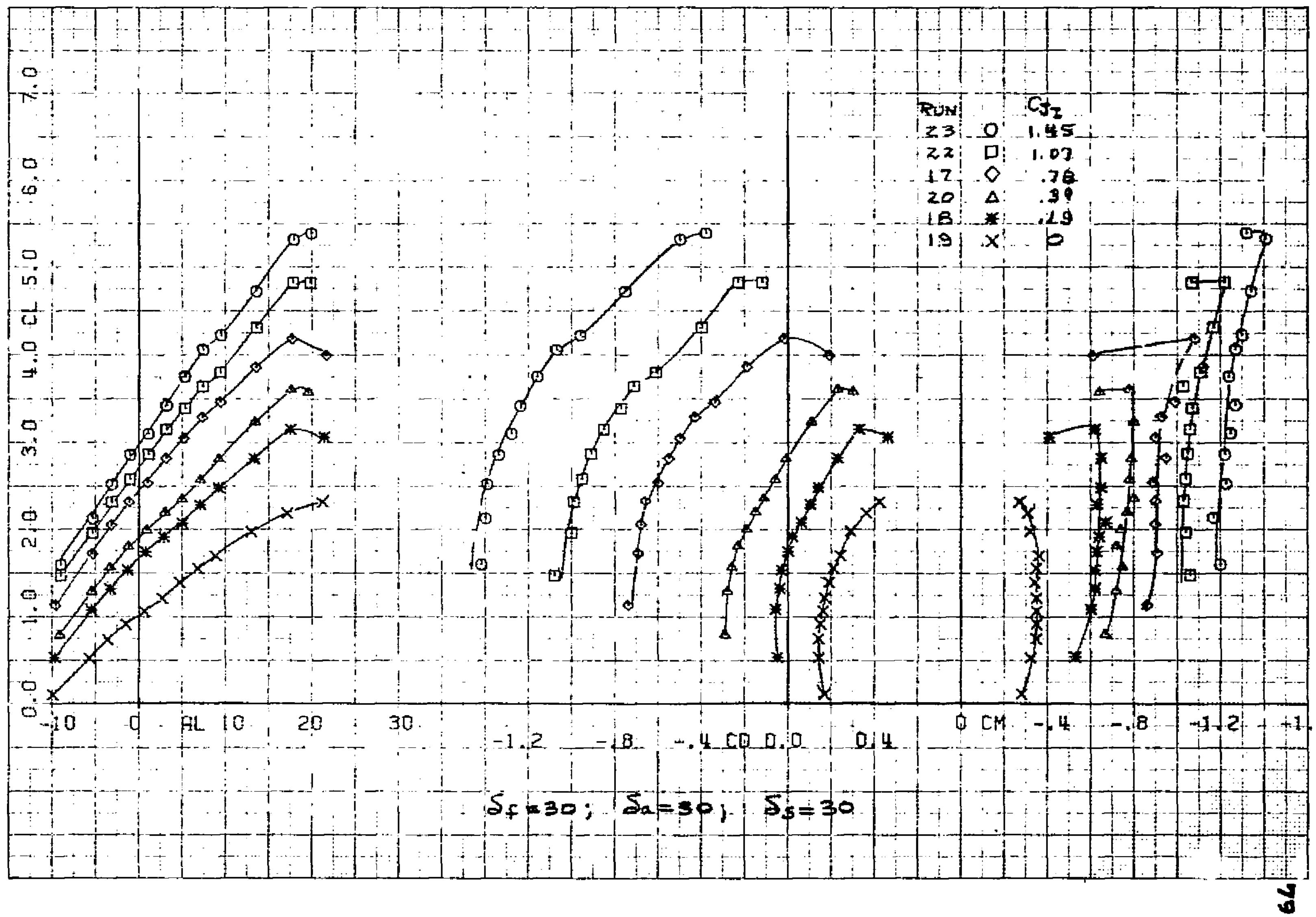

Figure 9.- Characteristics with the shroud and leading-edge slat on; δ_f, δ_a, and δ_s, 30°.

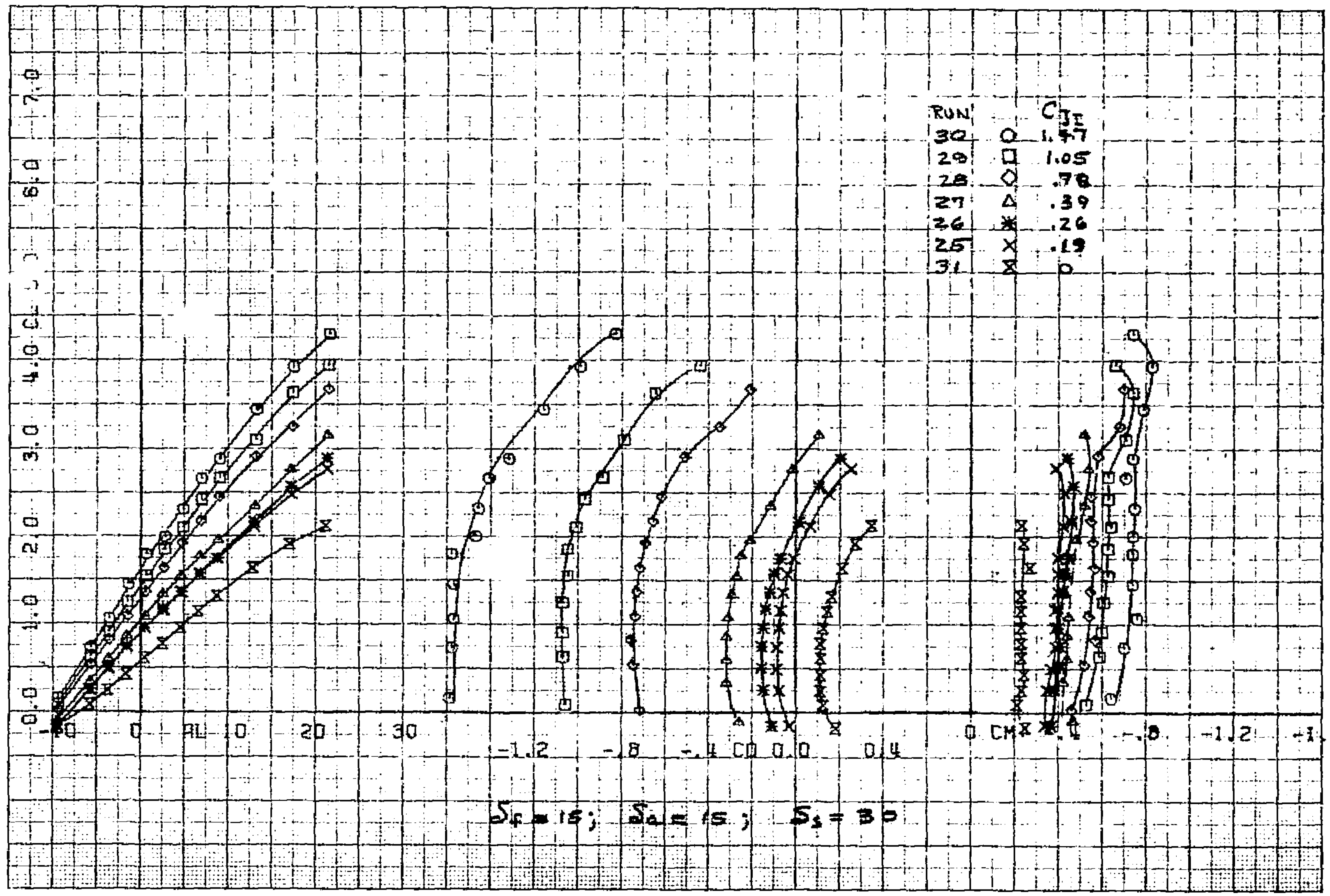

Figure 10.- Characteristics with the hroud and leading-edge slat on; δ_f and δ_a, 15°; δ_s, 30°.

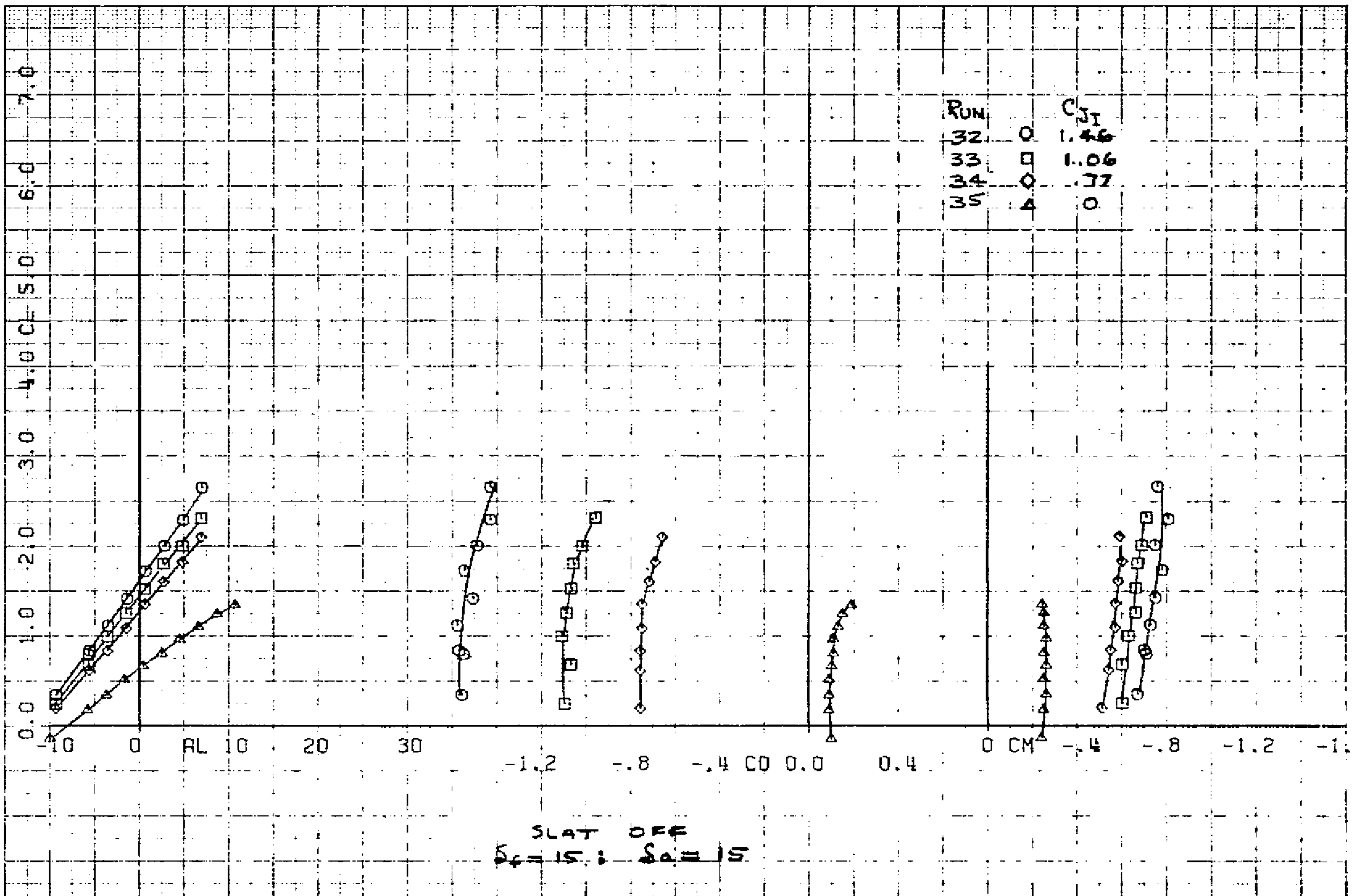

Figure 11.- Characteristics with the shroud on and leading-edge slat off; δ_f and δ_a, 15°.

ORIGINAL PAGE IS OF POOR QUALITY

81

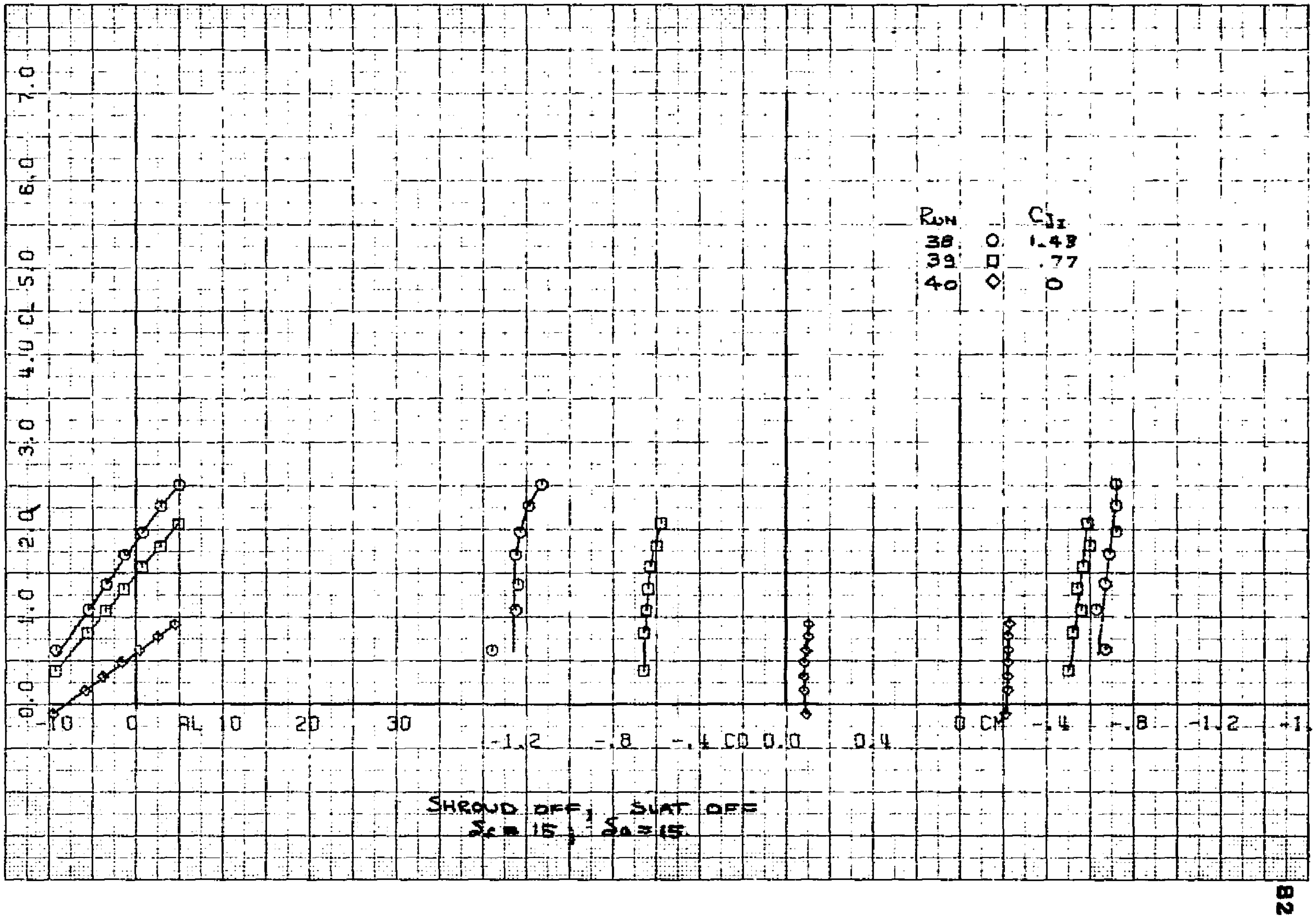

Figure 12.- Characteristics with the shroud and leading-edge slat off; δ_f and δ_s, 15°.

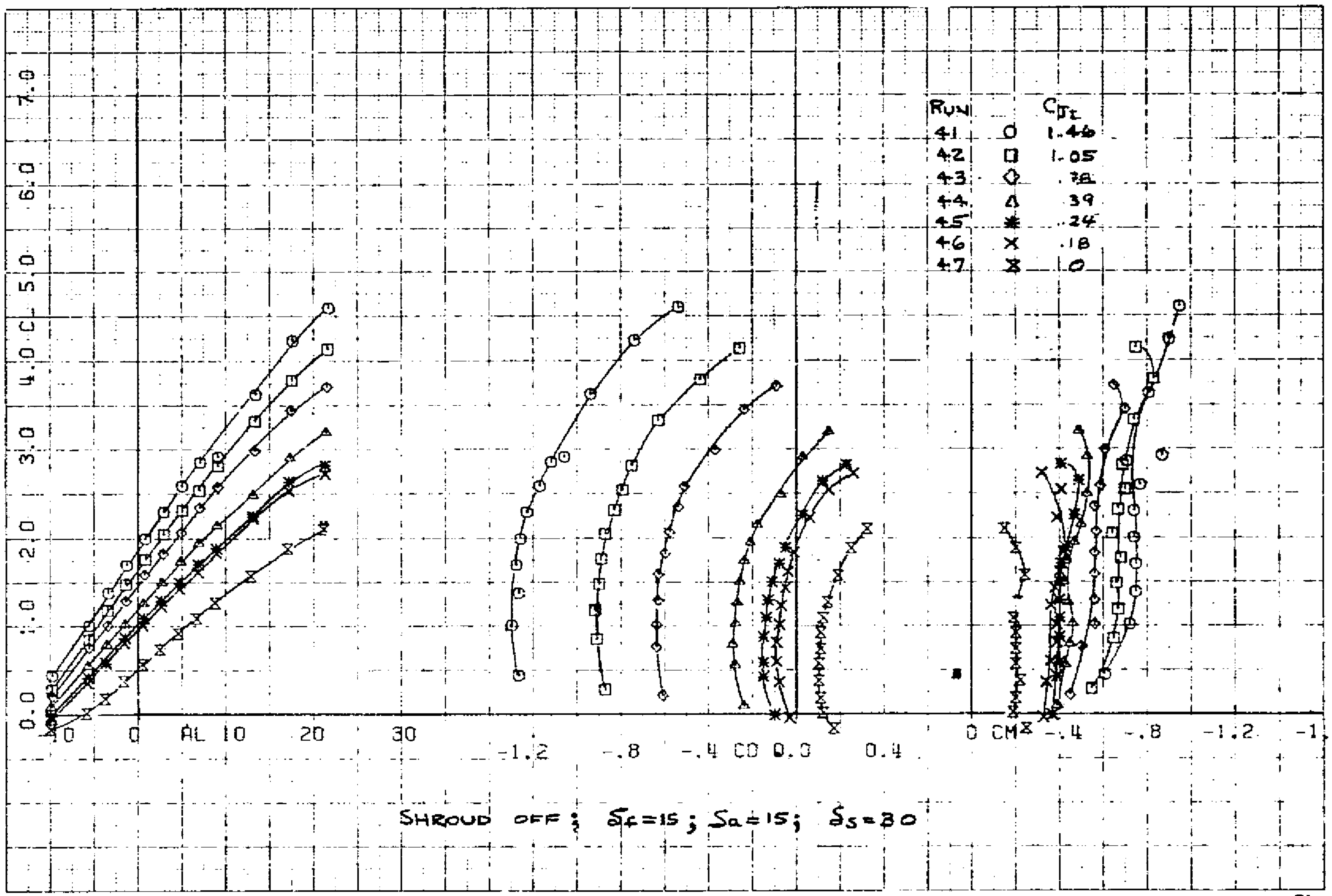

Figure 13.- Characteristics with the shroud off and leading-edge slat on; δ_f and δ_a, 15°; δ_s, 30°.

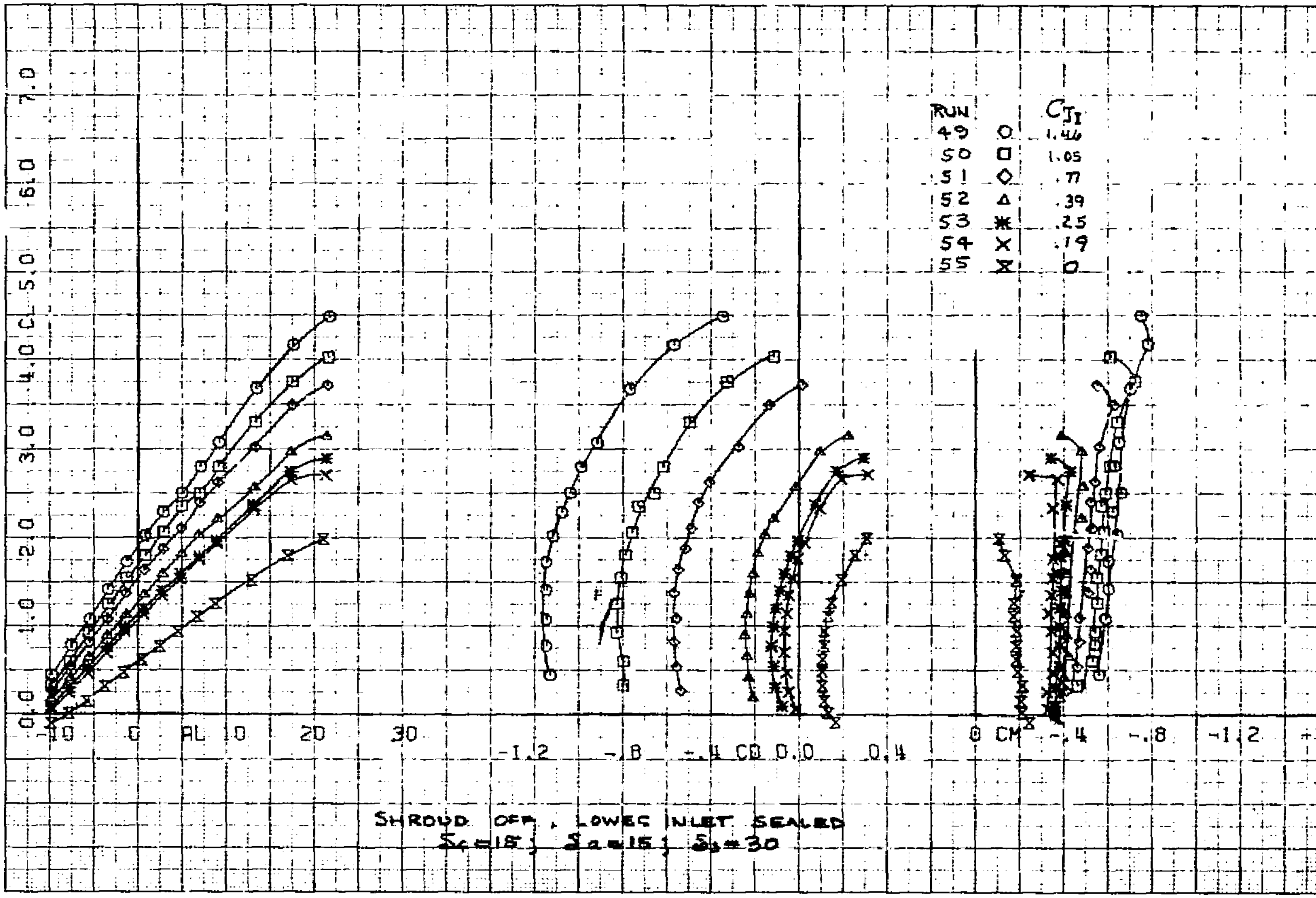

84

Figure 14.- Characteristics with the shroud off, slat on and the lower slot sealed; δ_f and δ_a, 15°; δ_s, 30°.

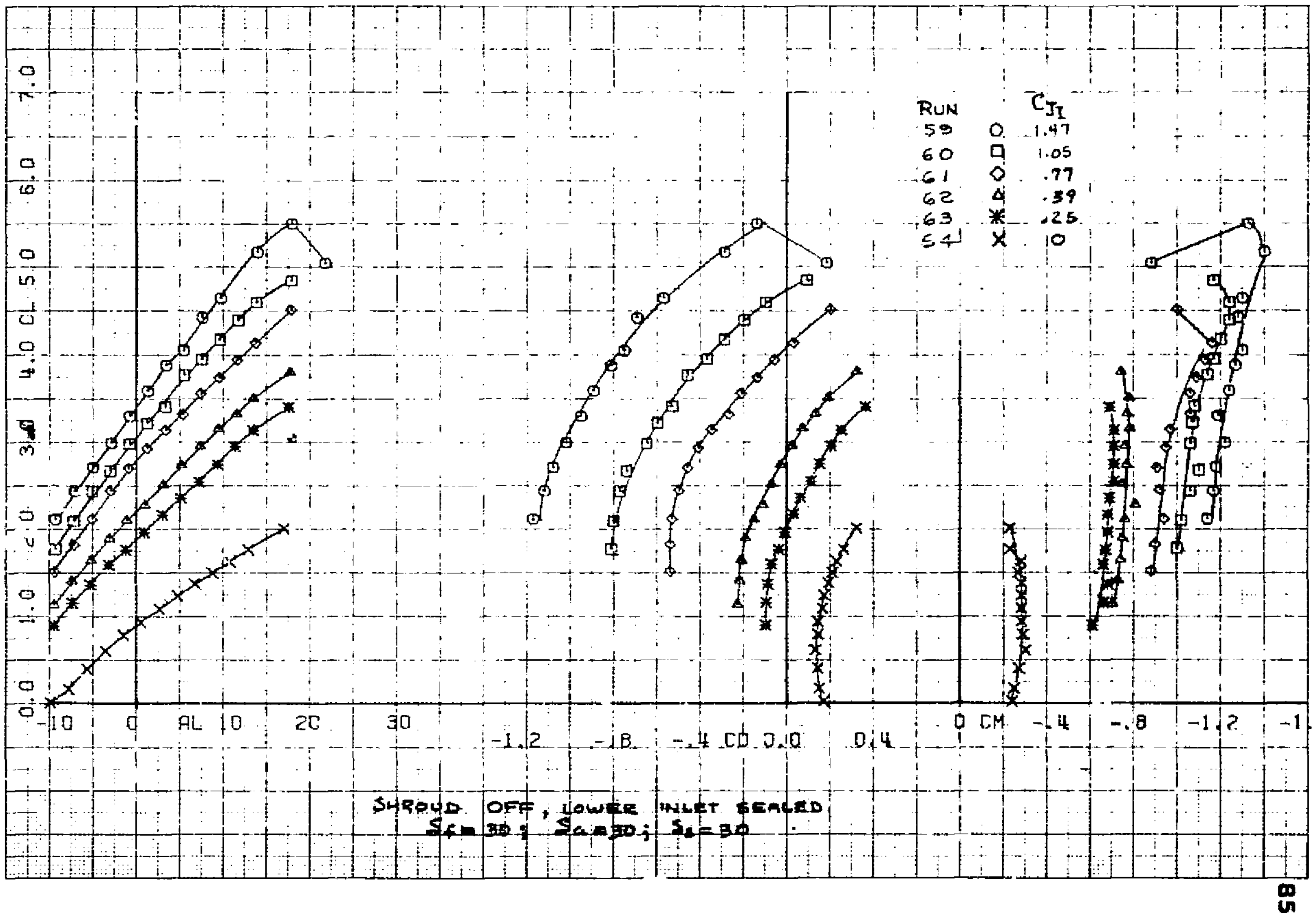

Figure 15.- Characteristics with the shroud off, slat on, and the lower slot sealed; δ_f, δ_a, and δ_s, 30°.

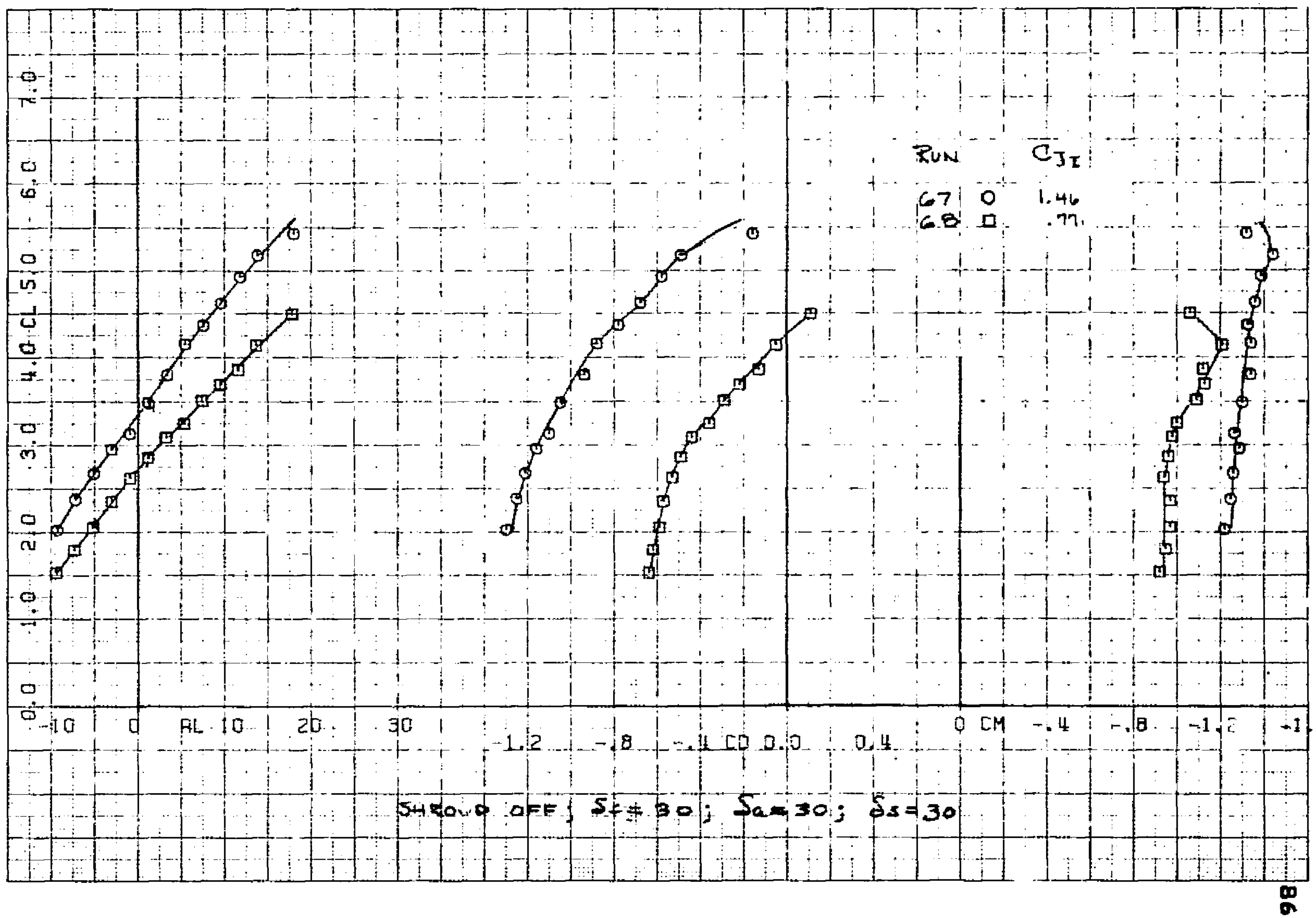

Figure 16.- Characteristics with the shroud off and leading-edge slat on; δ_f, δ_a, and δ_s, 30°.

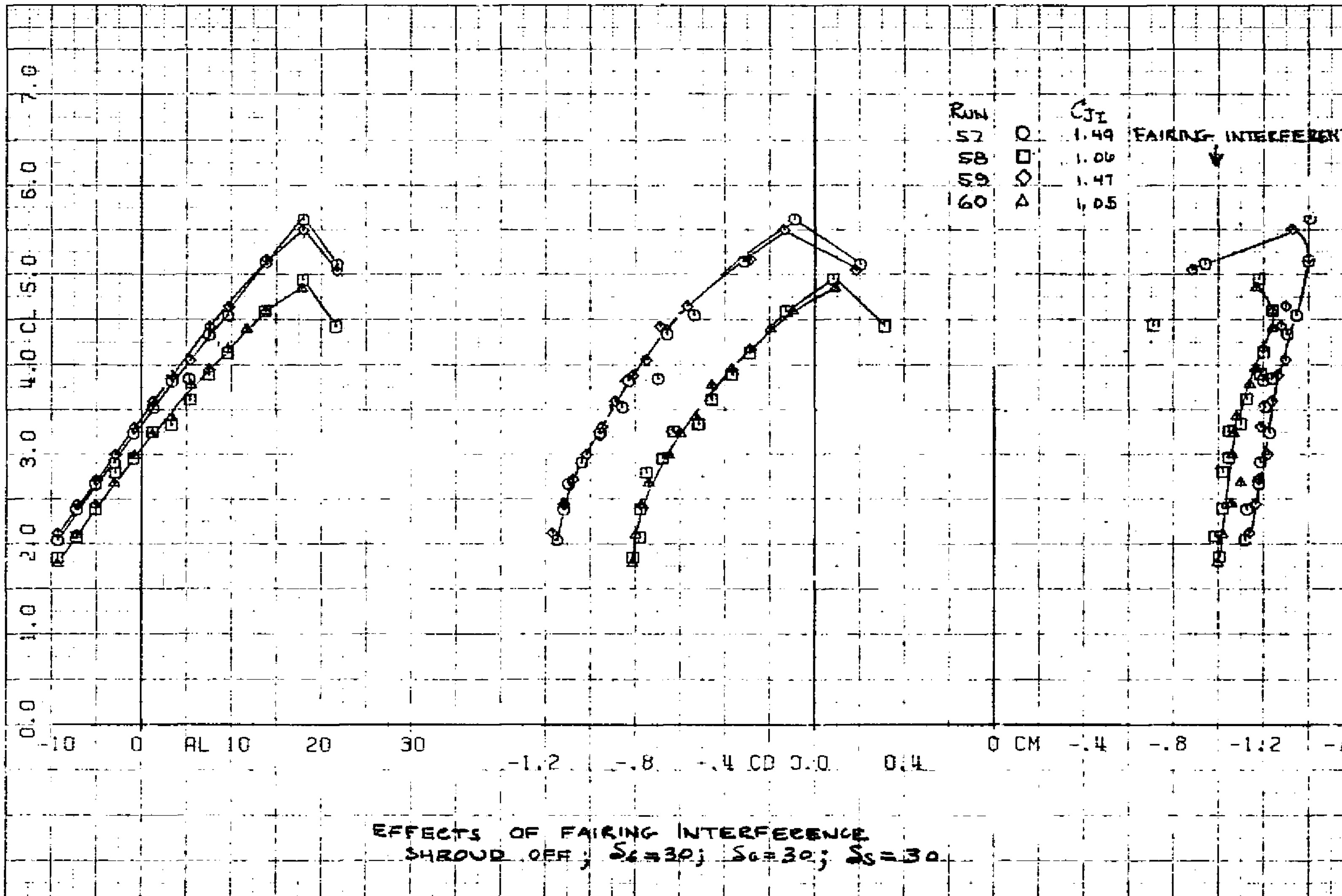

Figure 17.- The effect of support system mechanical interference (fouling); shroud off; slat on; slot sealed; δ_f, δ_a, and δ_s, 30°.

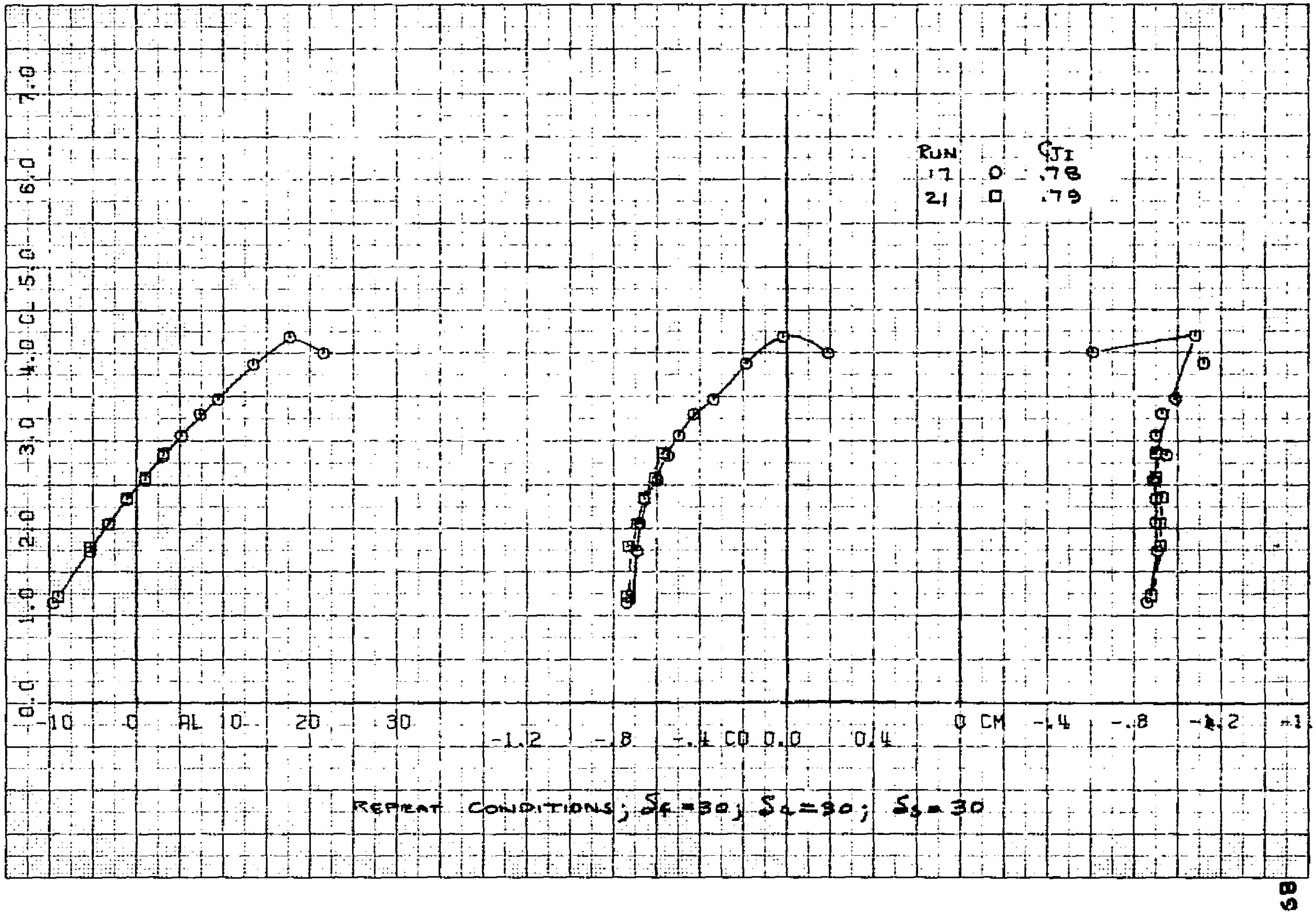

(a) $\delta_s = 30°$; repeat runs.

Figure 18.- Comparison of results of tests made at approximately the same test conditions; δ_f and δ_a, 30°.

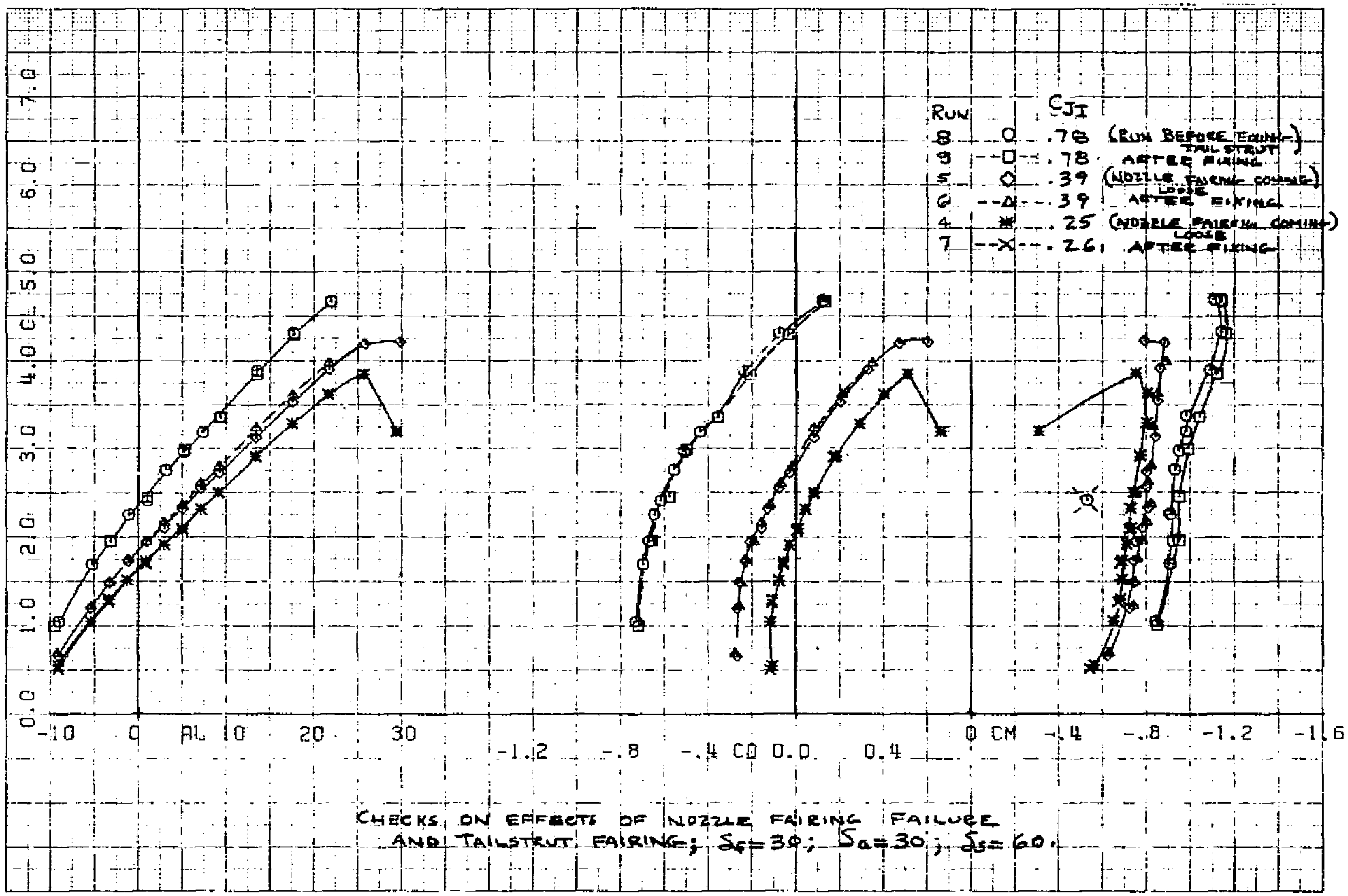

88

(b) $\delta_s = 60°$; effects of nozzle fairing and tailstrut failures.

Figure 18.- Concluded.

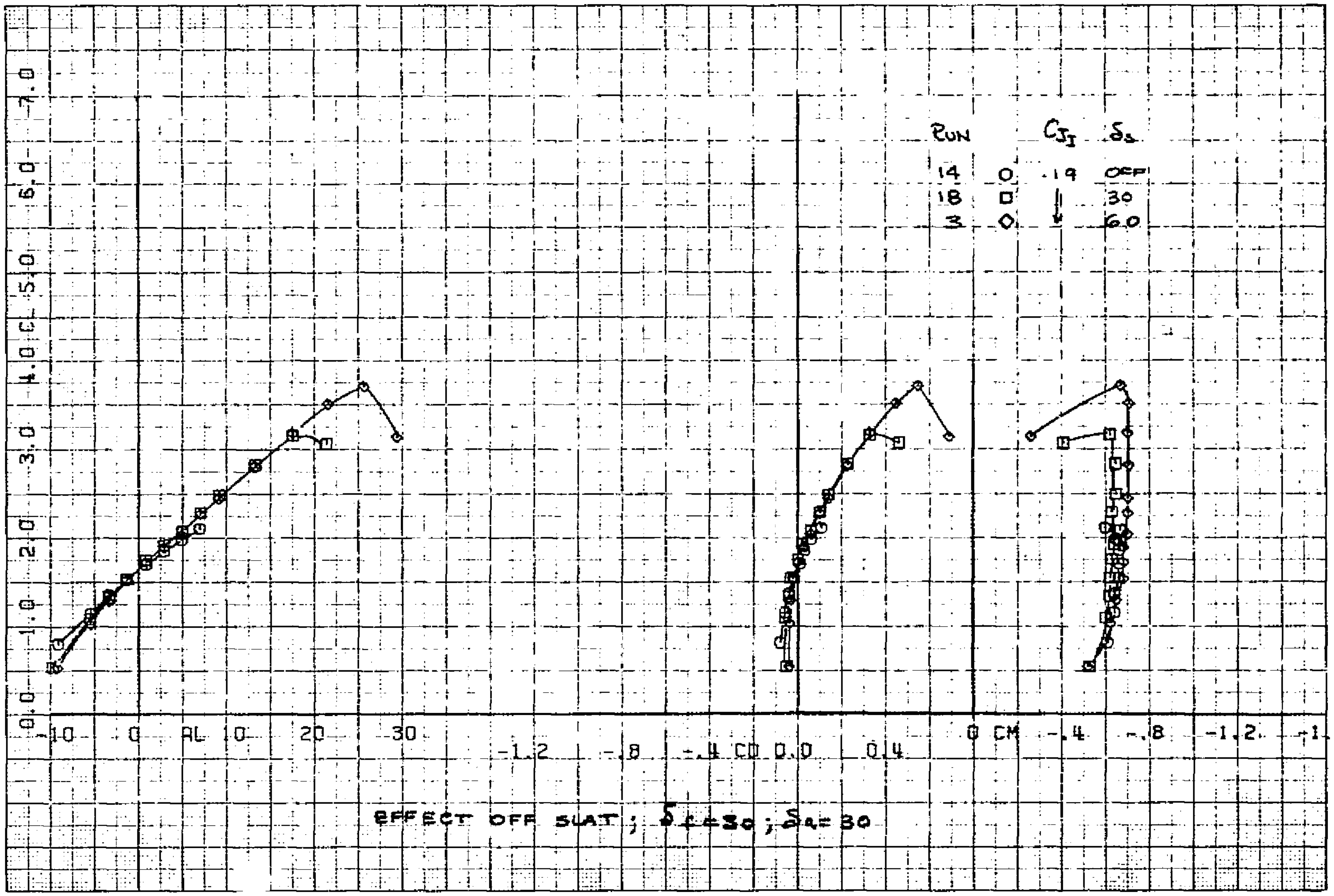

(a) δ_f and δ_a, 30°; C_J, 0.2.

Figure 19.- The effect of the leading-edge slat with shroud on.

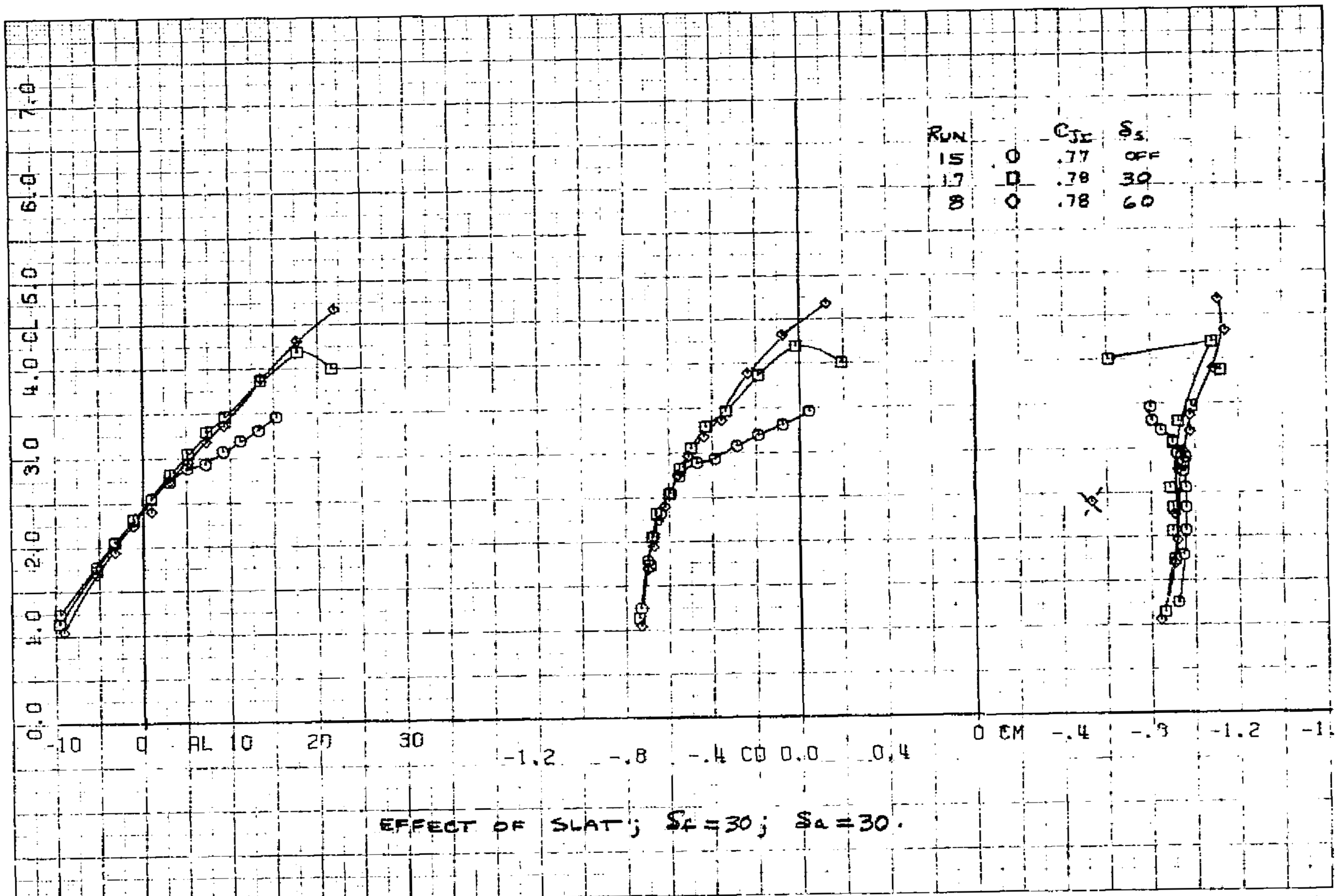

(b) δ_f and δ_a, 30°; C_J = 8.

Figure 19.- Continued.

ORIGINAL PAGE IS OF POOR QUALITY

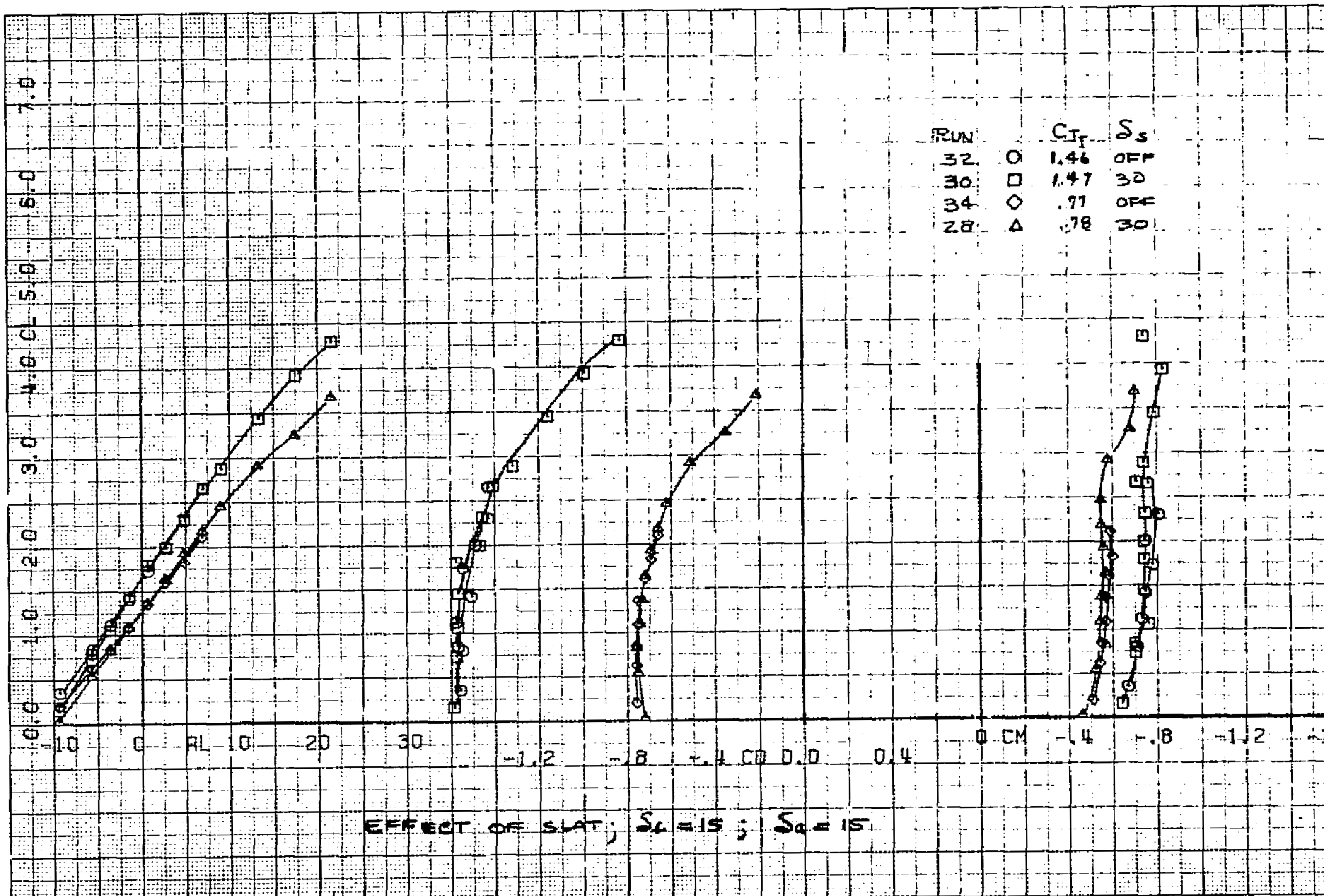

(c) δ_f and δ_a, 15°.

Figure 19.- Concluded.

47

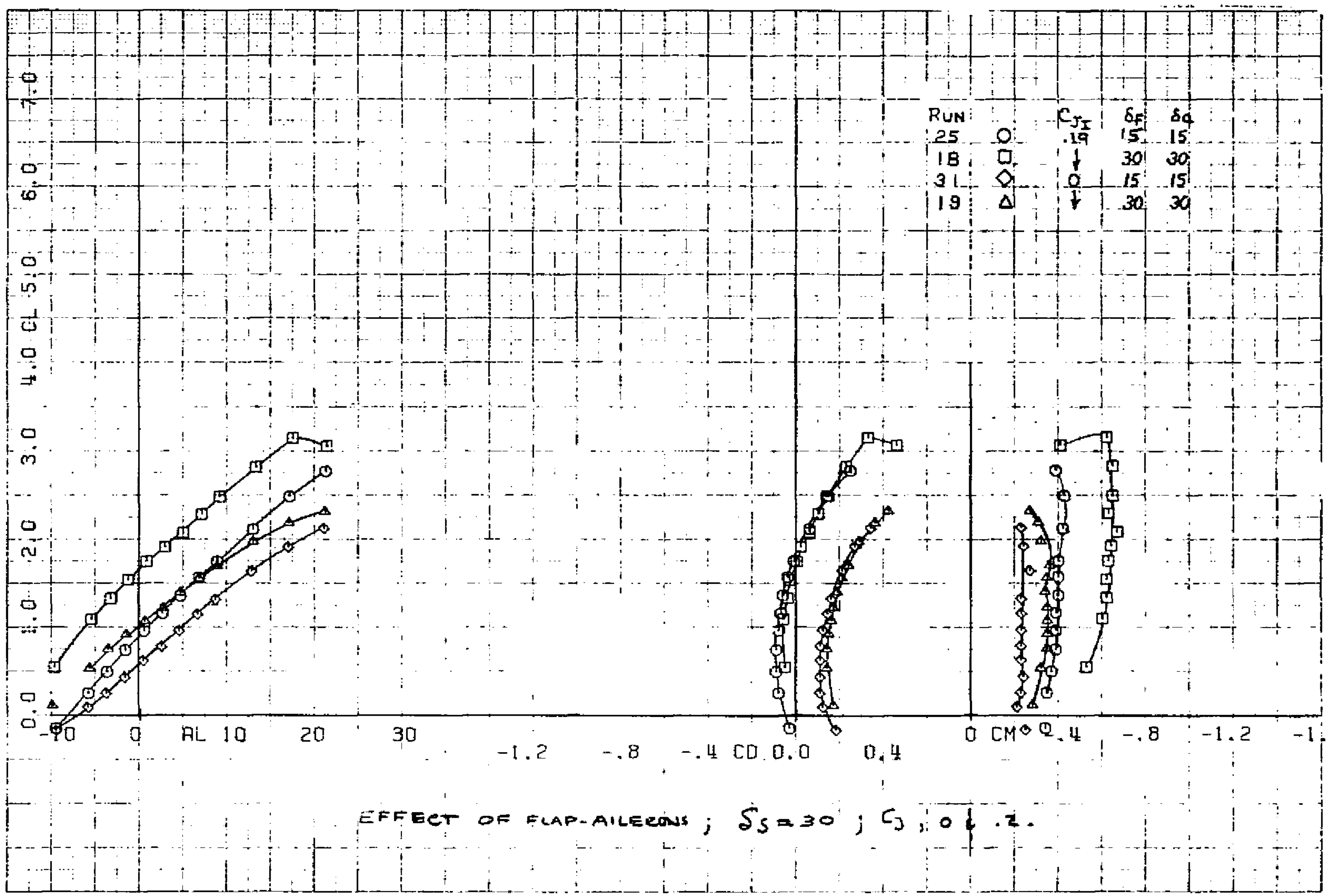

94

(a) C_J, 0 and 0.2.

Figure 20.- The effect of flap-aileron deflection with shroud on.

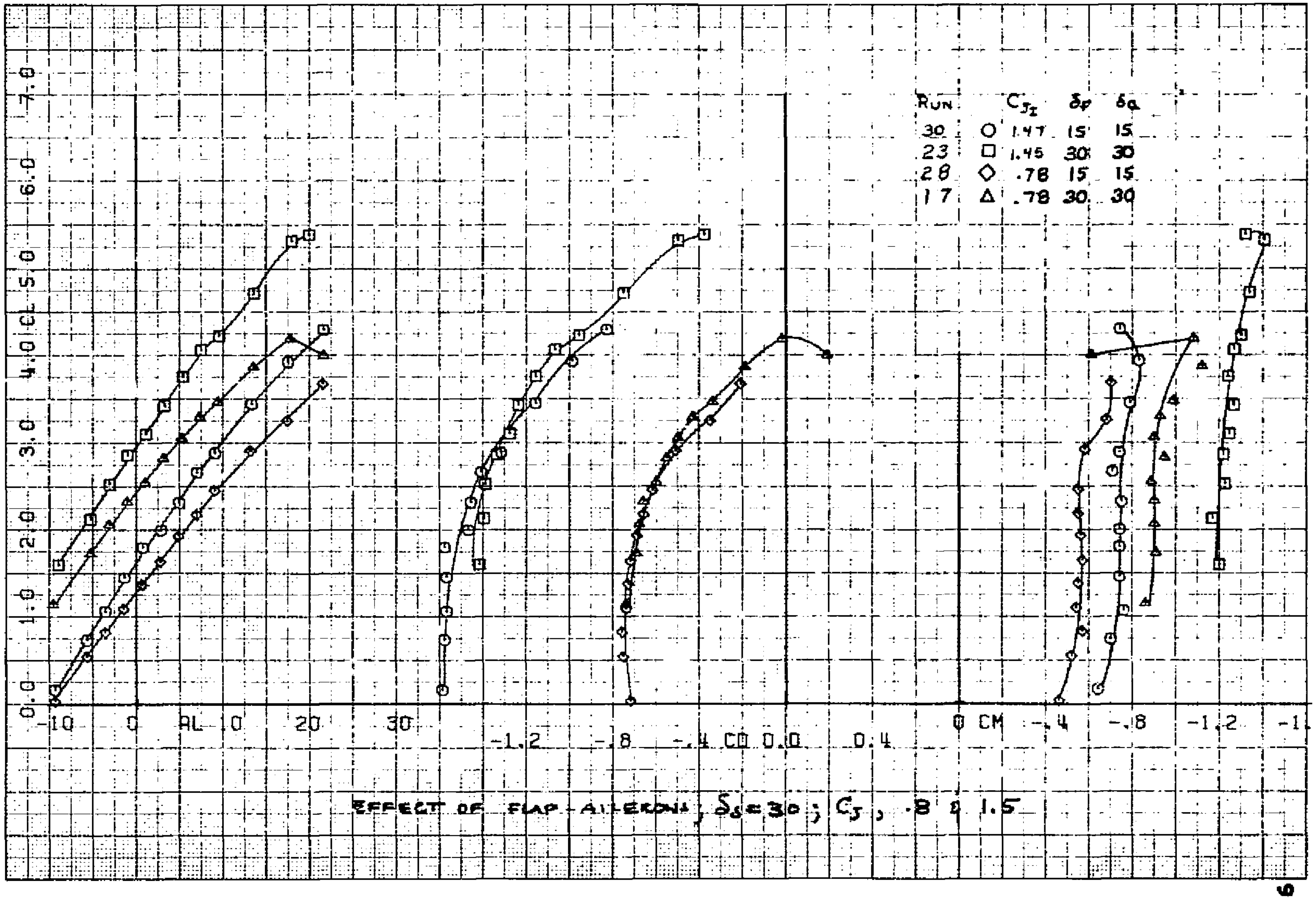

(b) C_J, 0.8 and 1.5.

Figure 20.- Concluded.

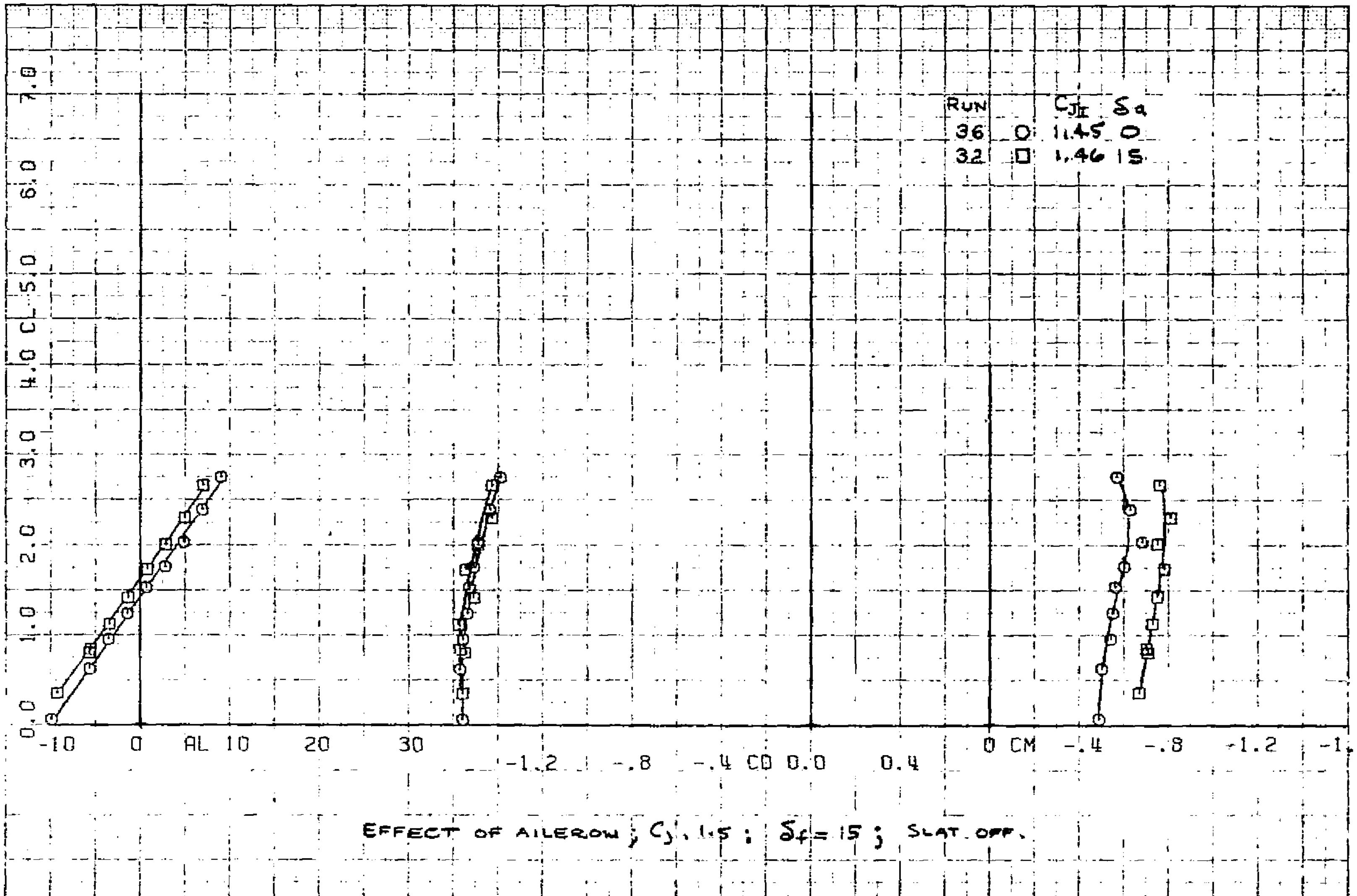

ORIGINAL PAGE IS
OF POOR QUALITY

Figure 21.- The effect of aileron deflection with slat off; δ_f, 15°; C_J, 1.5.

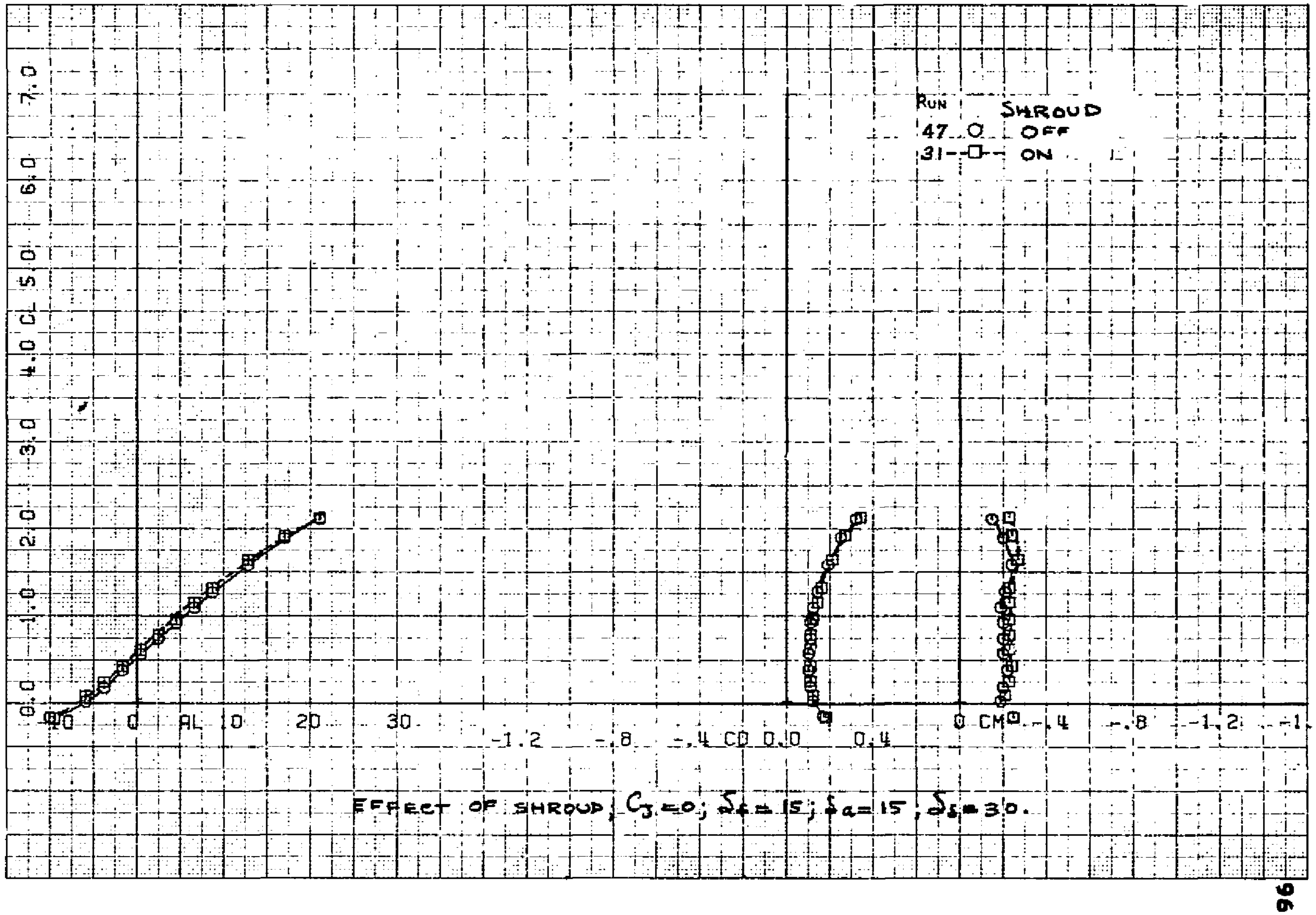

(a) δ_f and δ_a, 15°; C_J, 0.

Figure 22.- The effect of the shroud; δ_s = 30°.

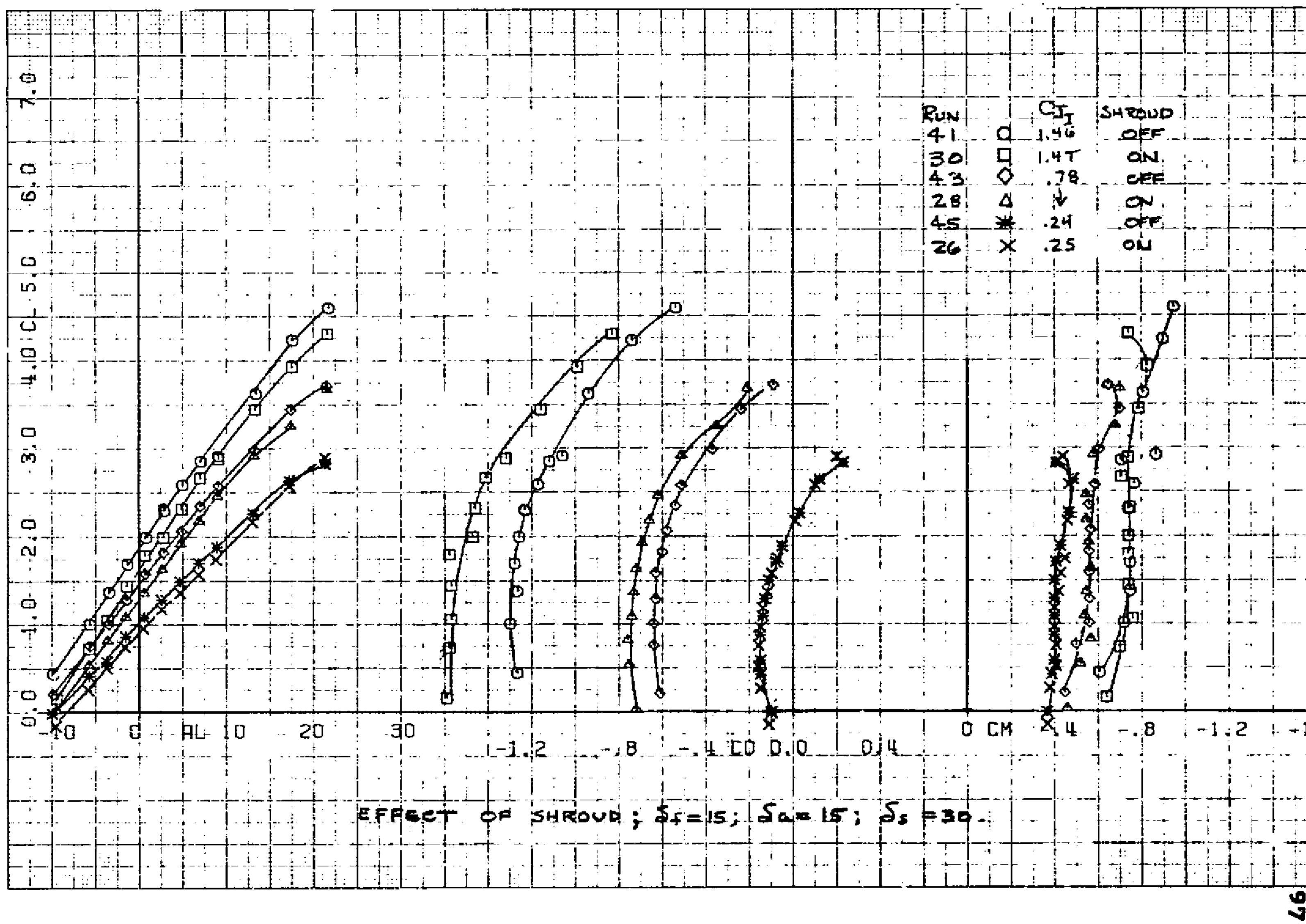

(b) δ_f and δ_a, 15°; C_J, 0.25, 0.8, and 1.5.

Figure 22.- Continued.

ORIGINAL PAGE IS OF POOR QUALITY

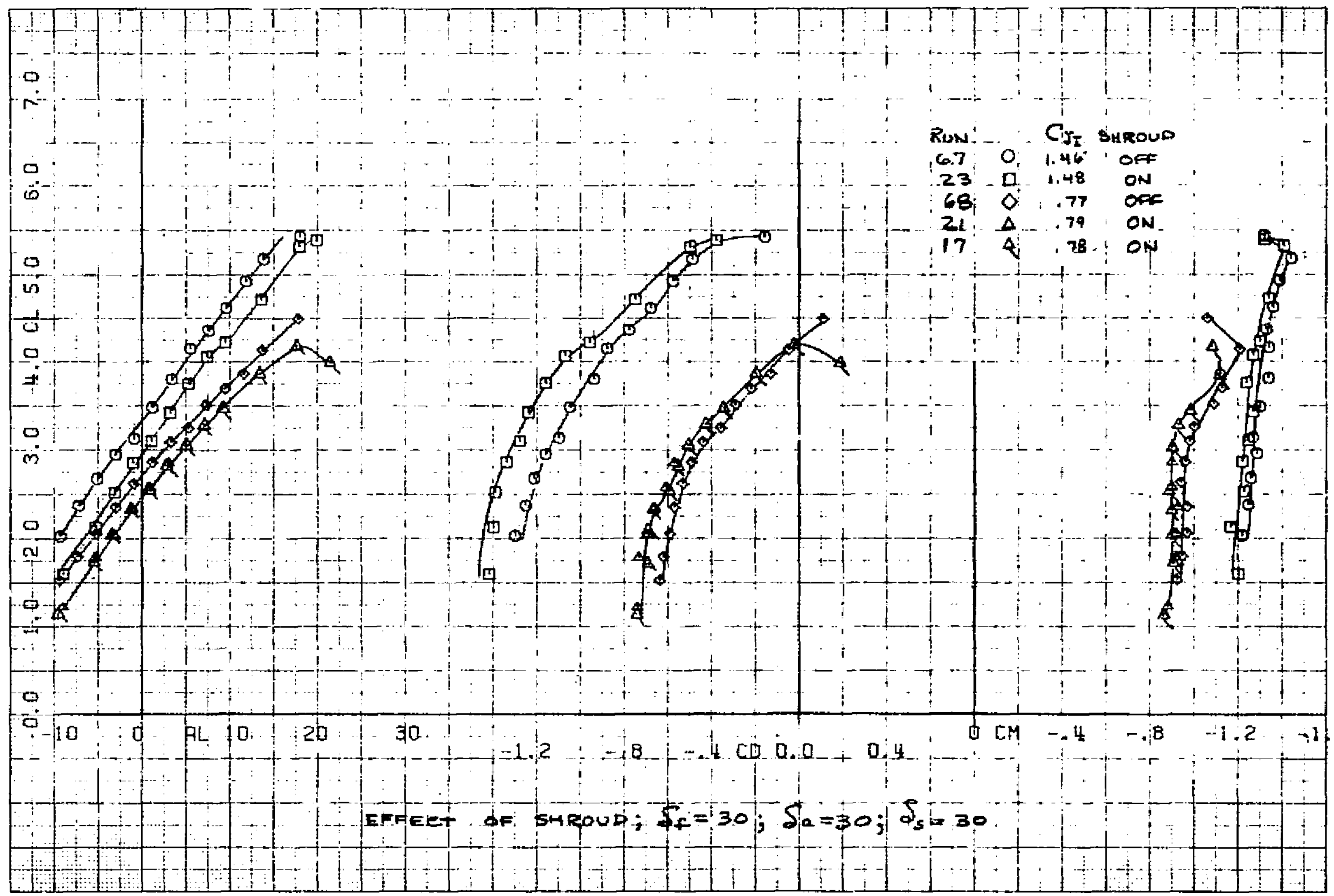

86

(c) δ_f and δ_a, 30°; C_J, 0.8 and 1.5.

Figure 22.- Concluded.

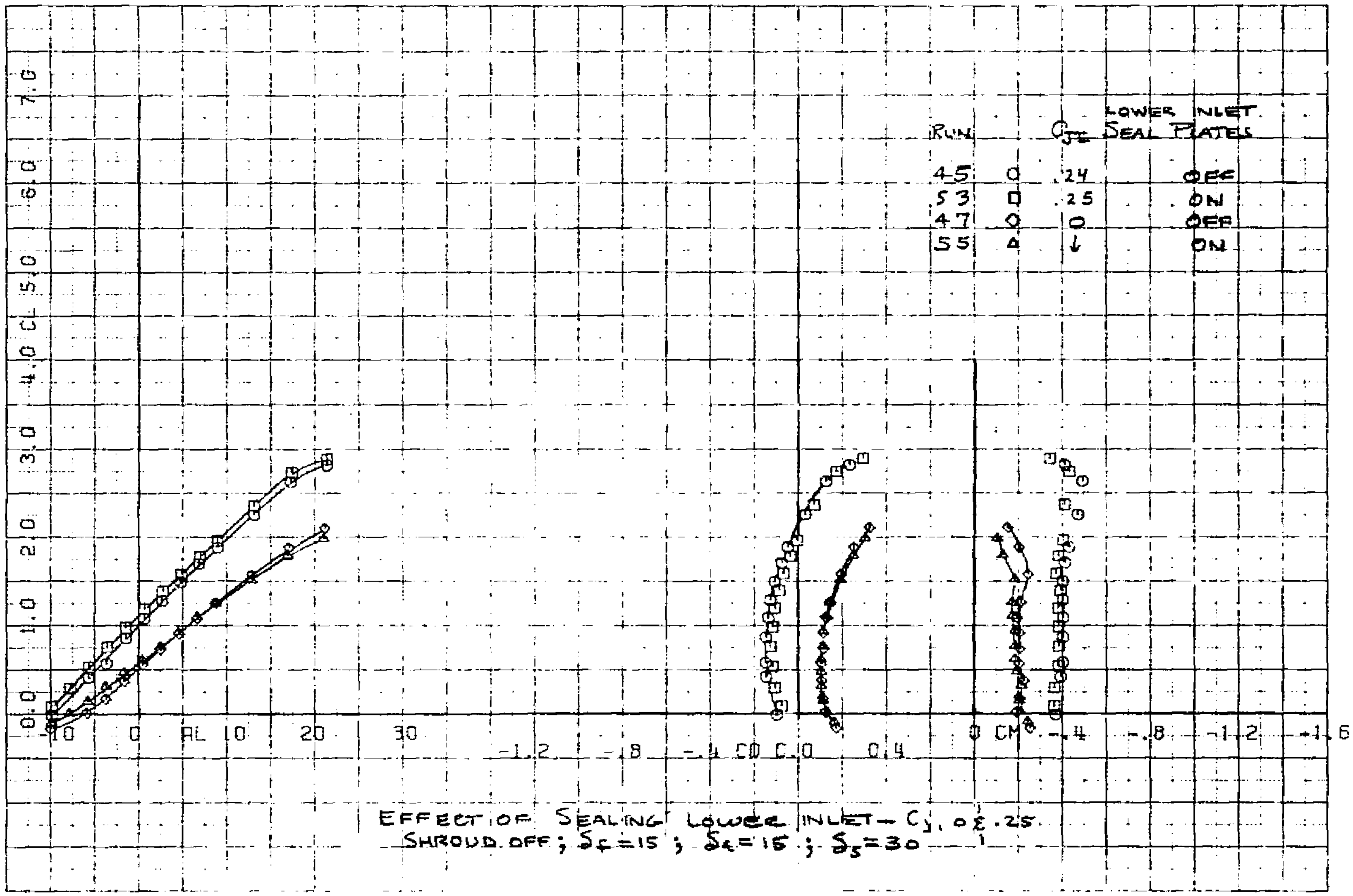

(a) δ_f and δ_a, 15°; C_J, 0 and 0.25.

Figure 23.- The effect of the lower slot seal; shroud off.

ORIGINAL PAGE IS OF POOR QUALITY

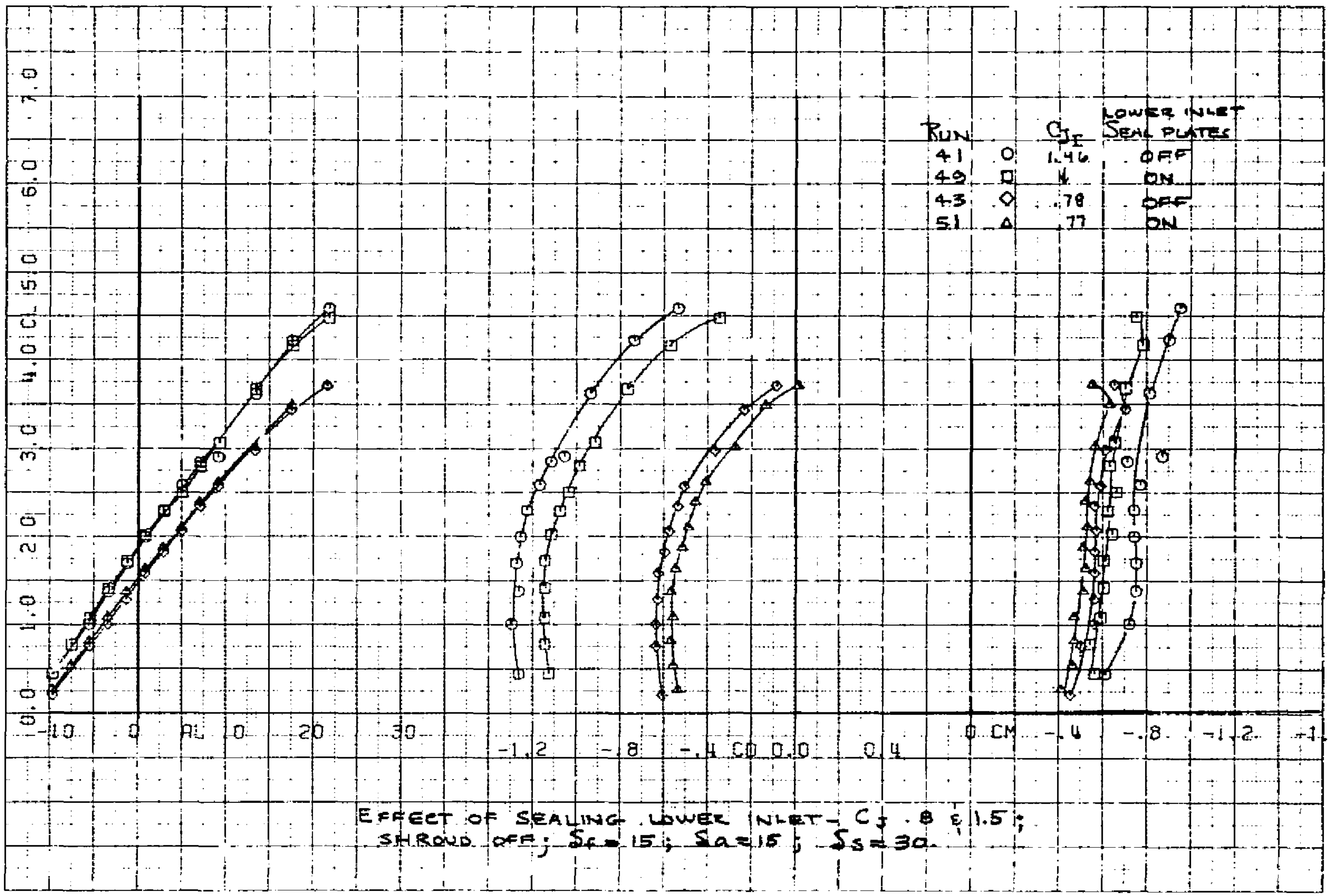

(b) δ_f and δ_a, 15°; C_J, 0.8 and 1.5.

Figure 23.- Continued.

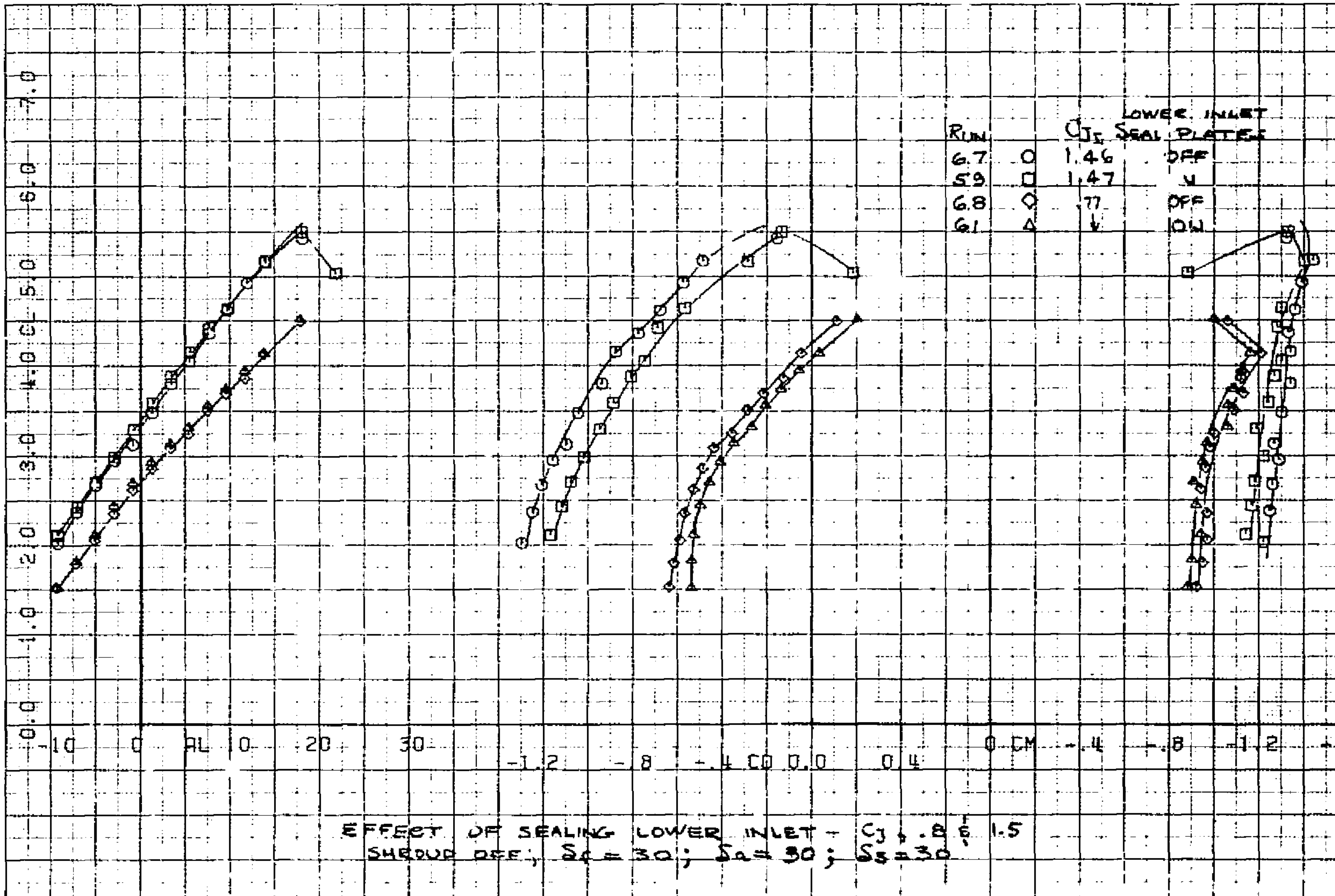

(c) δ_f and δ_a, 30°; C_J, 0.8 and 1.5.

Figure 23.- Concluded.